Scilight

Materials and Sustainability

https://www.sciltp.com/journals/matsus

Review

Additive Engineering in Crystallization Regulation of Highly Efficient Perovskite Solar Cell

Muhammad Arslan [1], Molang Cai [1,*], Xing Li [2], Xianggang Chen [1], Zhuoxin Li [1] and Aboubacar Traore [1]

[1] School of New Energy, North China Electric Power University, Beijing 102206, China
[2] Institute of Microelectronics, Chinese Academy of Science, Beijing 100029, China
* Correspondence: molangcai@ncepu.edu.cn

How To Cite: Arslan, M.; Cai, M.; Li, X.; et al. Additive Engineering in Crystallization Regulation of Highly Efficient Perovskite Solar Cell. *Materials and Sustainability* **2025**, *1*(4), 13. https://doi.org/10.53941/matsus.2025.100013

Received: 10 September 2025
Revised: 28 September 2025
Accepted: 8 October 2025
Published: 17 October 2025

Abstract: Metal halide perovskites are promising solar cell materials due to excellent photoelectric performance. High-quality films are crucial for stable perovskite solar cells (PSCs). However, defects, pinholes, and small grains hinder fabrication, causing nonradiative recombination. Among crystallization regulation strategies, additive engineering is versatile and effective for optimizing film quality via crystal growth control. This review summarizes the role of additive engineering in modulating crystallization across different perovskite types. For formamidinium (FA)-based perovskites, additives address problems like rapid crystallization, unstable secondary phases, residual stress, and random orientation, thereby stabilizing the phase and reducing grain boundaries. For methylammonium (MA)-based perovskites, additives (e.g., Lewis base-containing compounds and biomass-derived cellulose derivatives) adjust the lattice structure, slow down crystallization through intermediate adducts, and enhance grain alignment and defect healing. For all-inorganic $CsPbX_3$, additives (e.g., alkylamines and liquid monomers) decelerate crystallization to enlarge grains, decrease roughness through ion coordination, and form hydrophobic grain boundaries. Mechanistically, additives adjust crystallization kinetics, passivate defects via ion coordination, relieve residual stress, and direct preferential growth. This review offers insights for scalable high-quality film fabrication—essential for PSC commercialization—with future exploration of additives is set to further unlock PSC performance.

Keywords: additives engineering; crystal growth; high-efficiency PSCs

1. Introduction

Organic–inorganic metal halide perovskites have rapidly revolutionized the photovoltaic (PV) industry since their emergence in 2009. Perovskite solar cells (PSCs) have achieved record power conversion efficiencies (PCEs) of 27% in single-junction devices, which is close to the best performance of crystalline silicon solar cells (27.3%), and have attained an even higher 34.85% in perovskite/silicon tandem structures [1–3]. Such remarkable progress is attributed to the inherent optoelectronic traits of perovskites, such as their strong light absorption, long carrier diffusion lengths, tunable bandgap, low exciton binding energy, and the ability to form high-quality crystalline films routes at relatively low-cost using solution-based or vapor-assisted fabrication.

However, despite these achievements, commercialization of PSCs remains hindered by low reproducibility of device performance and intrinsic instability. The root cause lies in the uncontrollable, rapid, and random crystallization kinetics that occur during film formation, which often leads to films that have poor surface coverage, pinholes, residual stress, and heterogeneous grain boundaries. These flaws expedite degradation and act as non-radiative recombination centers, and thus restrict both efficiency and long-term stability. Therefore, the main

challenge is to precisely regulate the crystallization process to achieve dense, uniform, and defect-minimized high quality perovskite films.

To address this challenge, various approaches have been researched, such as substrate modification, solvent/anti-solvent engineering, post-treatments, and additive incorporation. Among them, additive engineering has emerged as one of the most adaptable and effective approaches, because of the structural and functional diversity of available additives [4–6]. Additives ranging from polymers, solvents, and fullerenes to inorganic/organic salts, acids, and nanoparticles can modulate the kinetics of nucleation and growth, passivate bulk and interfacial defects, inhibit ion migration, and improve charge transport, thereby enabling the fabrication of high-quality perovskite films [7–10].

While the utility of specific additives is well-documented in focused studies, the literature lacks a thorough and systematic analysis that links the chemical functionality of additives to their mechanistic role in regulating crystallization across the entire spectrum of perovskite material classes. Existing reviews often categorize additives by their chemical type (e.g., polymers, salts) rather than by the specific crystallization challenge they address (e.g., phase stabilization, stress relief, orientation control, Sn^{2+} oxidation) for different perovskites (e.g., FA-based, MA-based, inorganic, Sn-based). This gap prevents a holistic understanding of structure–function relationships and hinders the rational design of next-generation additives.

This review aims to fill that critical gap. We provide a targeted overview of additive engineering strategies, uniquely organized around the key crystallization challenges in various perovskite systems. We meticulously analyze how different categories of additives—tailored for formamidinium (FA), methylammonium (MA), all-inorganic $CsPbX_3$, tin (Sn), antimony (Sb), and 2D perovskites—mechanistically regulate film growth, minimize defects, and enhance device performance and durability. By synthesizing knowledge across these material platforms, this review offers unique insights into the design principles of multifunctional additives, providing a valuable guide for the scalable fabrication of high-quality perovskite films—an essential step toward the ultimate commercialization of perovskite photovoltaics.

2. Additive in FA-Based Perovskite

The Formamidinium lead iodide ($FAPbI_3$) has gradually taken the place of the first widely used methylammonium lead iodide ($MAPbI_3$) [11]. $FAPbI_3$ is thermally more stable than $MAPbI_3$, which degrades more rapidly under heat and moisture. And $FAPbI_3$ has a bandgap 1.48 eV closer to the Shockley-Queisser limit, this allows $FAPbI_3$ to absorb more of the solar spectrum, especially near-infrared light, enhancing efficiency, moreover, $FAPbI_3$ films often form larger grains and fewer grain boundaries than $MAPbI_3$, leading to lower charge recombination, better charge carrier mobility, higher open-circuit voltage (V_{oc}) and fill factor (FF) which makes it the most appealing perovskite layer for single-junction PSCs [12,13]. However, $FAPbI_3$ perovskite still suffers from inferior quality, which poses a significant obstacle to achieving higher efficiency. We discuss here the different mechanisms behind the additive engineering to influence the crystal growth of $FAPbI_3$ perovskite film. The performance of FA-based PSCs utilizing a selection of additives is benchmarked in Table 1.

2.1. Additive for Controlling Crystallization Rate

Generally, the perovskite quality is mainly controlled by nucleation and crystal growth [14–16]. In the first stage of perovskite film formation, the monomers initially accumulate in the solution. With the increase in the monomer concentration, a supersaturation environment is created and monomers become arranged in a pattern characteristic of a crystalline solid, forming nuclei. In the next stage upon the formation of nuclei, additional particles are deposited upon the nuclei as the crystal growth subsequently happens, accompanied by further nucleation in the meantime. Nucleation is terminated when the concentration of monomers is lower than the critical supersaturation value. Eventually, the crystal growth will be finalized when the concentration of monomers decreases below the solubility value. If nucleation is fast, many crystals form nearly simultaneously. Thus, the majority of crystals grow to approximately identical uniform sizes. In contrast, if nucleation is slow and fewer crystals nucleate at a time, the supersaturation in the solution drops slowly, the nucleation of new crystals continues, and a population of crystals of various sizes forms. Regarding the crystal growth process, the much faster crystal growth rate in comparison to nucleation tends to bring the centralized growth of the crystal. This, as a result, will lead to the formation of pin-holes and disordered grains. Whereas, excessively slow growth can lead to phase segregation (e.g., in mixed halides). Thus, the fast nucleation (to ensure uniform seeding) followed by moderate, controlled crystal growth rate (to allow well-ordered, defect-minimized grains) is ideal for high-quality perovskite films [17–21].

Therefore, it is required to appropriately control and modulate the crystallization rate by rationally tuning the strength of the chemical interaction between additives and perovskite precursor compositions. Additives contribute to extra homogeneous nucleation sites and slow down the perovskite crystallization by forming an intermediate adduct with PbI_2, which allows the randomly formed nuclei to adjust their orientation [22]. In this aspect, Cao et al. employed dimethylformamide (DFA) as an additive in the $FAPbI_3$-based perovskite precursor solutions for the fabrication of PSCs [23]. In this process, DFA reacts with DMSO, leading to the formation of Dimethyl thiethane (MEADTE) and Dimethyl acetamide (DA). The functional groups C=O and -S- in DTE, along with the C=O group in DA, can interact with lead iodide. These bonds have high binding energies stronger than the original DMSO-PbI_2 bond, effectively creating a more stable complex and effectively slow down the crystallization process during the formation of perovskite films. Consequently, resulting in good quality with larger grains, better orientation, and fewer defects Figure 1a. By delaying the crystallization kinetics of the perovskite film, the addition of DFA to the precursor solution boosted the average PCE of PSCs from 22.64% to 24.74%, with a peak PCE of 25.28%. The reduction in defects and improvement in film quality contributed to the enhanced stability of the PSC, which retained 95.75% of its initial PCE after 1152 h. Wang et al. used the multifunctional additive Lansoprazole (Lanz) in $FAPbI_3$ perovskite precursor solution which retards the crystallization process of the perovskite film through molecular interaction [24]. The sulfinyl moiety (>S=O) on the Lanz molecule is a strong electron donor, which allows it to coordinate with and bind to the lead ions (Pb^{2+}) in the precursor solution. This coordination forms transient complexes that slow down the reaction kinetics between lead and iodide ions, thereby delaying crystal growth phases. This results in a slower transformation of the precursor film into the final crystalline perovskite structure, as evidenced by the observed delay in the film turning black during annealing. This results in larger grains (from 0.75 μm to 0.91 μm) and reduced grain boundaries, as observed in SEM images Figure 1b. The trifluoromethyl ($-CF_3$) group in Lanz additive forms a hydrophobic barrier on the surface can also provide moisture oxygen stability and sulfinyl group passivate defects by coordinating with dangling Pb^{+}. Lanz also adjust the Fermi-level of PCS film, thereby optimizing the energy match between functional layers, which unhindered the separation, extraction, and transport of carriers. The Lanz-modified device achieved an excellent PCE of 24.05%, as well as exceptional environmental and operational stability like sustains 84% of its original efficiency under a continuous irradiation (100 mW cm^{-2}) for 500 h.

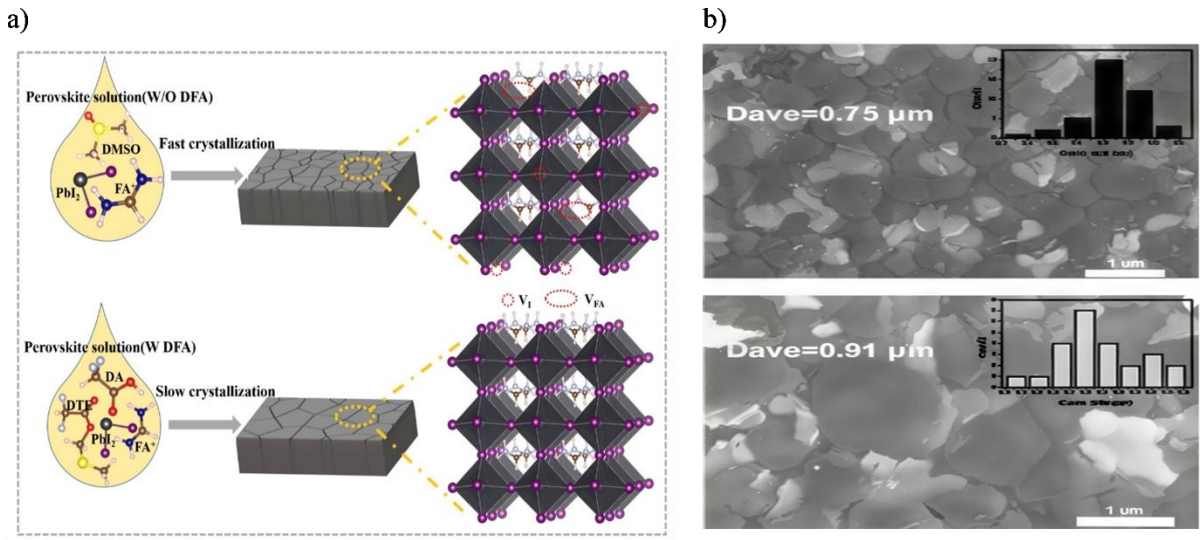

Figure 1. (**a**) The fast and slow crystallization process of perovskite film prepared without and with DFA additive. Reproduced with permission [23]. Copyright 2024, Angewandte Chemie int. Ed. (**b**) Top view SEM images of pristine and Lanz modified perovskite films. Reproduced with permission [24]. Copyright 2022, Chemical Engineering Journal.

2.2. Additive for α Phase Stabilization

The black, cubic α-phase of formamidinium lead iodide ($FAPbI_3$) is the keystone of high-performance perovskite solar cells due to its superior optoelectronic properties, including a near-ideal bandgap of ~1.45–1.48 eV for broad sunlight absorption, exceptional thermal stability from the large FA^{+} cation, and superior charge transport. However, a critical challenge is that this high-performing α-phase is metastable at room temperature. Its thermodynamically favoured state is actually a yellow hexagonal δ-phase, a transition driven by an intrinsic instability

where the large FA^+ cation is more stable in the non-perovskite δ-phase lattice. This detrimental shift is readily stimulated by moisture, strain, or simply over time. The resulting δ-phase is a wide-bandgap, optically inactive semiconductor that cannot absorb sunlight effectively, rendering a solar cell powerless. Therefore, the central pursuit in advancing $FAPbI_3$ photovoltaics is not just exploiting the advantages of the black α-phase, but actively stabilizing it against its inevitable conversion to the useless yellow phase. To overcome this, strategic additives are employed to permanently stabilize the α-phase. These additives, such as smaller cations like Cs^+ or MA^+, work by incorporating into the crystal lattice to optimize its tolerance factor and strain, thereby making the black phase thermodynamically favourable. Simultaneously, passivating additives like potassium iodide (KI) segregate at grain boundaries to suppress ion migration and passivate defects that initiate decomposition. Therefore, the use of these additives is essential to kinetically trap and thermodynamically favour the functional black phase, preventing its conversion to the yellow phase and enabling the realization of $FAPbI_3$'s full potential for high-efficiency and stable photovoltaics. In this regard, Wang et al. incorporated a trace amount of PTAC (3% vol) which significantly stabilizes the α-phase without forming a 2D perovskite layer [25]. It acts primarily as a strain relaxer and defect passivator. The electron-rich benzene ring in PTAC acts as a Lewis base, coordinating with under-coordinated Pb^{2+} ions (Lewis acids) at grain boundaries and surfaces. This coordination saturates dangling bonds, reducing the density of trap states that often act as nucleation points for the δ-phase. This coordination also effectively "caps" the stress sites. The bulky benzene ring physically pushes the surrounding iodide ions slightly apart, causing a local expansion of the crystal lattice. This local expansion directly counteracts the pervasive tensile strain that was pulling the lattice taut. Figure 2a Grazing incidence X-ray diffraction (GIXRD) data proving the release of micro-strain. For the control film, the X-ray diffraction (XRD) peak shifts to lower angles with increasing incidence angle, indicating gradient tensile strain through the film depth. For the PTAC-modified (P3) film, the peak position remains constant, showing a homogenous, strain-free lattice. A relaxed lattice is less prone to phase transition. Simultaneously, the increased work function of modulated film optimizes the band alignment, promoting carrier transport and reducing nonradiative recombination, thereby improving the open- circuit voltages and fill factors. Consequently, the champion device achieved a power conversion efficiency of 24.51% and demonstrated exceptional operational stability, retaining 90% of its initial performance after 1000 h of continuous illumination. Wang et al. used MACl and $PbCl_2$ dual additive synergism which thermodynamically stabilizes the α-phase by drastically lowering its formation energy, enabling its direct formation and suppressing the δ-phase from the very beginning of crystallization [26]. The MA molecules intercalate into the perovskite precursor lattice, forming a low-energy intermediate phase (e.g., $MA_2PbI_{8-x}Cl_x$ DMSO). This temporary structure acts as a "scaffold" that templates the crystallization of the perovskite, reducing the energy required to form the α-phase upon annealing. The Cl^- from both additives incorporates into the lattice, further stabilizing the α-phase structure and simultaneously raising the energy barrier for the formation of the undesirable δ-phase. Figure 2b DFT calculation bar chart showing the formation energy of α-$FAPbI_3$ is lowest with the dual additive, explaining why the direct formation occurs. The resulting inverted perovskite solar cells achieved a high efficiency of 26.17% and demonstrated excellent shelf stability, retaining 93% of their initial performance after 2000 h in ambient air.

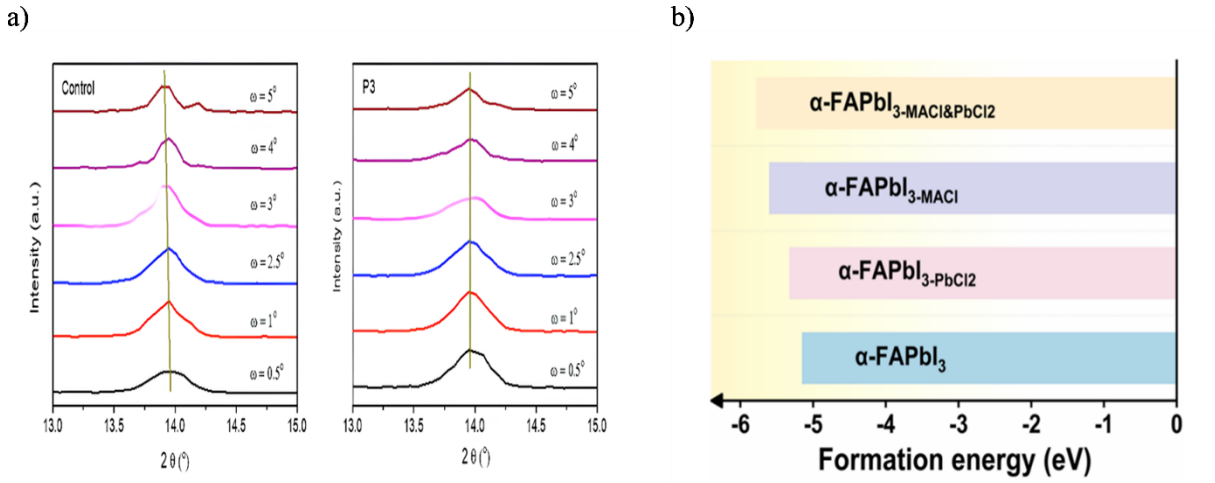

Figure 2. (**a**) GIXRD patterns with different ω 4 values (0.5°–5°) for control and P3 perovskite films. Reproduced with permission [25]. Copyright 2024, Nano Energy (**b**) Synergism revealing formation energy. Reproduced with permission [26]. Copyright 2025, Chemical Engineering Journal.

2.3. Additive for Excess PbI_2 Free Crystal Growth

Many reports have demonstrated that small amount of excess PbI_2 is valuable for achieving high performance [27]. The benefits of small amount of excess PbI_2, whether it is present at the grain boundary or in the bulk of perovskite films have mainly been attributed to its passivation effect, which is the result of the formation of a type-I band alignment and improves carrier lifetime, suppressing non-radiative recombination, eliminates hysteresis effect and slightly boosting V_{OC} and FF and eventually build high-performance levels of PSCs [28,29]. However, too much of excess PbI_2 in $FAPbI_3$ perovskite is fundamentally detrimental because it directly undermines the material's stability and electronic properties. Firstly, PbI_2 is highly hygroscopic, that means it readily absorbs moisture from the air. This absorbed water then initiates and speeds up the decomposition of the surrounding perovskite film, reverting the stable black phase back into its constituents and causing fast performance degradation. Secondly, while a small amount can passivate defects, an excess of this insulating compound creates barriers within the film that hinder the smooth transport of electrical charges. This forces photo-generated electrons and holes to recombine at the interfaces between the perovskite and PbI_2 domains, a process that wastes energy as heat and significantly reduces the device's voltage and power output. Thirdly, a significant amount of unreacted PbI_2 is a clear indicator of an incomplete conversion process, resulting in a non-uniform film with a mixed phase composition and poor morphology that is riddled with pinholes and defects. Finally, these PbI_2-rich regions and the defective grain boundaries they create provide pathways for harmful ion migration, which is a primary cause of current-voltage hysteresis and long-term operational instability, making the device's performance unpredictable and unreliable over time. To achieve high efficiency, it is essential to control unstable excess PbI_2 in perovskite films. Zhao et al. proposed RbCl additive doping can transform excess PbI_2 into an inactive $(PbI_2)_2RbCl$ compound, effectively stabilizing the perovskite phase [30]. During the perovskite film fabrication, RbCl is added to the precursor solution. As the film crystallizes, rubidium (Rb^+) ions, due to their small ionic radius, do not efficiently incorporate into the $FAPbI_3$ perovskite lattice (the A-site is too large for them). Instead, they tend to segregate towards the grain boundaries and surfaces, which are also the locations where unreacted excess PbI_2 tends to accumulate. A solid-state reaction occurs where the RbCl molecules coordinate with PbI_2 forming a more complex, stabilized $(PbI_2)_2RbCl$ compound which is electronically inert and chemically stable and less hygroscopic. This removes the primary pathway for moisture ingress that leads to perovskite decomposition. In Figure 3a Scanning electron microscopy (SEM) shows the perovskite film crystallinity improved. As the control film, the perovskite crystal grain size was ~1 mm, and the grains were surrounded by PbI_2 grains (white needle shapes,), which formed as decomposition products on the perovskite surface after heating at elevated temperatures. For the RbCl doped films, the perovskite crystal size was increased to ~2 mm. The numerous, distinct needle-like PbI_2 structures have disappeared and replaced by a few sporadic, irregular white flakes. These flakes are the new, inactive $(PbI_2)_2RbCl$ compound. The resultant $FaPbI_3$ perovskite film attained PCE of 25.6% with almost hysteresis-free. Luo introduced melamine (MEA) as an additive to regulate PbI_2 concentration in sequentially deposited perovskite films [31]. MEA's donor-acceptor structure interacts with PbI_2's surface: its triazine core binds to uncoordinated lead, while amino groups coordinate with iodide, passivating defects and enhancing carrier separation Figure 3b. Combined with cesium iodide, MEA also improved perovskite crystallization, increased (111) orientation, and reduced pinholes. This synergy enabled inverted PSCs with a PCE of 25.66%. Wang developed natural cellulose derivatives to manage effect of excess PbI_2 [32]. The cationic derivative C-Im-CN has multiple functional groups (imidazolium cation, cyano group, hydroxyl group, carbonyl group, and chloride anion) which strongly interact with perovskite components via electrostatic, coordination, and hydrogen-bonding interactions. These interactions promote the transfer of excess PbI_2 from grain boundaries to the surface of perovskite grains or its aggregation into plate-like crystallites in local domains. This redistribution suppresses defect formation, reduces grain boundary defects, and inhibits the degradation of perovskite under environmental stresses, thereby enhancing both the efficiency 24.71% PCE and stability of the solar cells.

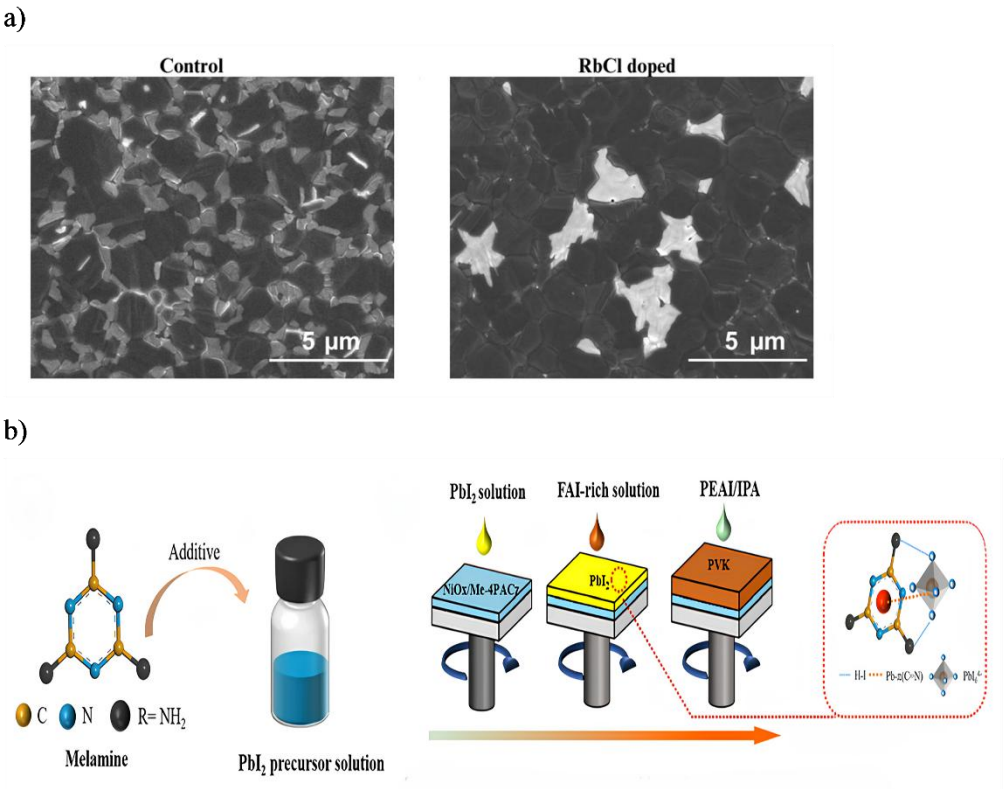

Figure 3. (**a**) SEM of perovskite films without RbCl and with 5% RbCl, respectively. Scale bars, 5 mm. Reproduced with permission [30]. Copyright 2022, Solar Cells (**b**) Chemical structure of MEA and Schematic illustration of preparation process of inverted PSCs by sequential deposition method and tridentate chelation to PbI_2. Reproduced with permission [31]. Copyright 2025, Royal Society of Chemistry.

2.4. Additives for Residual Stress-Free Crystal Growth

The residual stress in perovskite film, which originates from local lattice mismatch, misorientation, the volumetric shrinkage from solvent loss, and thermal expansion coefficient difference between perovskite and substrate. This residual stress must be carefully considered due to its significant impact on defect formation, carrier transport, and ion migration [33–35]. Releasing residual stress is thought to significantly increase the effectiveness and stability of PSC by effectively reducing interface recombination and ionic migration. To overcome this challenge, Zuo employed cellulose diacetate (CDA), a sustainable material derived from plant fibers [36]. The hydroxyl (-OH) and carbonyl (C=O) functional groups in CDA strongly coordinate with PbI_2. This interaction passivates defects and reduces strain at the atomic level by forming Lewis acid-base adducts, which stabilize the perovskite lattice and minimize lattice distortions Figure 4a. Furthermore, CDA reduces the Young's modulus of the perovskite film, indicating enhanced mechanical compliance. This reduction in stiffness allows the film to better accommodate external and thermal stresses, thereby decreasing residual stress concentrations. This approach yielded a power conversion efficiency (PCE) of 24.68% on flexible substrates—among the highest reported for F-PSCs. Sun et al. develop a viable crystallization strategy for the two-step fabrication of $FAPbI_3$ by embedding thiourea and successfully controlling the residual stress [37]. The key mechanism involves the formation of an ultrathin, two-dimensional (2D) perovskite-like buffer layer at the heterojunction interface, which is facilitated by the bilateral affinity of thiourea. The functional groups in thiourea, namely the carbon-sulfur double bond (C=S) and amine groups ($–NH_2$), engage in strong Lewis acid-base coordination with undercoordinated Pb^{2+} ions from the perovskite and simultaneously interact with the SnO_2 substrate Figure 4b. This dual interaction creates a bridging bond that alleviates the lattice mismatch between the SnO_2 electron transport layer and the perovskite absorber layer, which is a primary source of residual tensile stress generated during film fabrication due to differences in thermal expansion coefficients and non-equilibrium crystallization. The incorporation of thiourea via a competitive crystallization strategy further modulates the perovskite growth dynamics. By pre-occupying the A-sites in the perovskite lattice during the two-step sequential deposition process, thiourea temporarily forms a $TuPbI_3$ or mixed-dimensional phase, which delays rapid nucleation and promotes the growth of larger, more oriented grains Figure 4c. This process reduces structural disorder and internal strain within the film. The thiourea-optimized device has shown the best efficiency of 24.42% and maintains over 80% after 120 h continuous

illumination at 60 °C. Li and coworkers designed a novel multifunctional additive, methylammonium succinate (MS) in which the two terminal carboxyl groups can form hydrogen bonds with formamidine (FA) with two neighbouring perovskite grains, while the flexible ethylene spacer helps relieve residual strain caused by residual stress, leading to perovskite films with reduced defects and enhanced durability Figure 4d [38]. Moreover, the carboxyl group can coordinate with the dangling Pb^{2+} present at the surface of perovskite grains, and the MA^{+} can compensate for the A position vacancy in the ABX_3 perovskite, reducing the number of defects. Consequently, achieved a high PCE of 23.6% for FPSC.

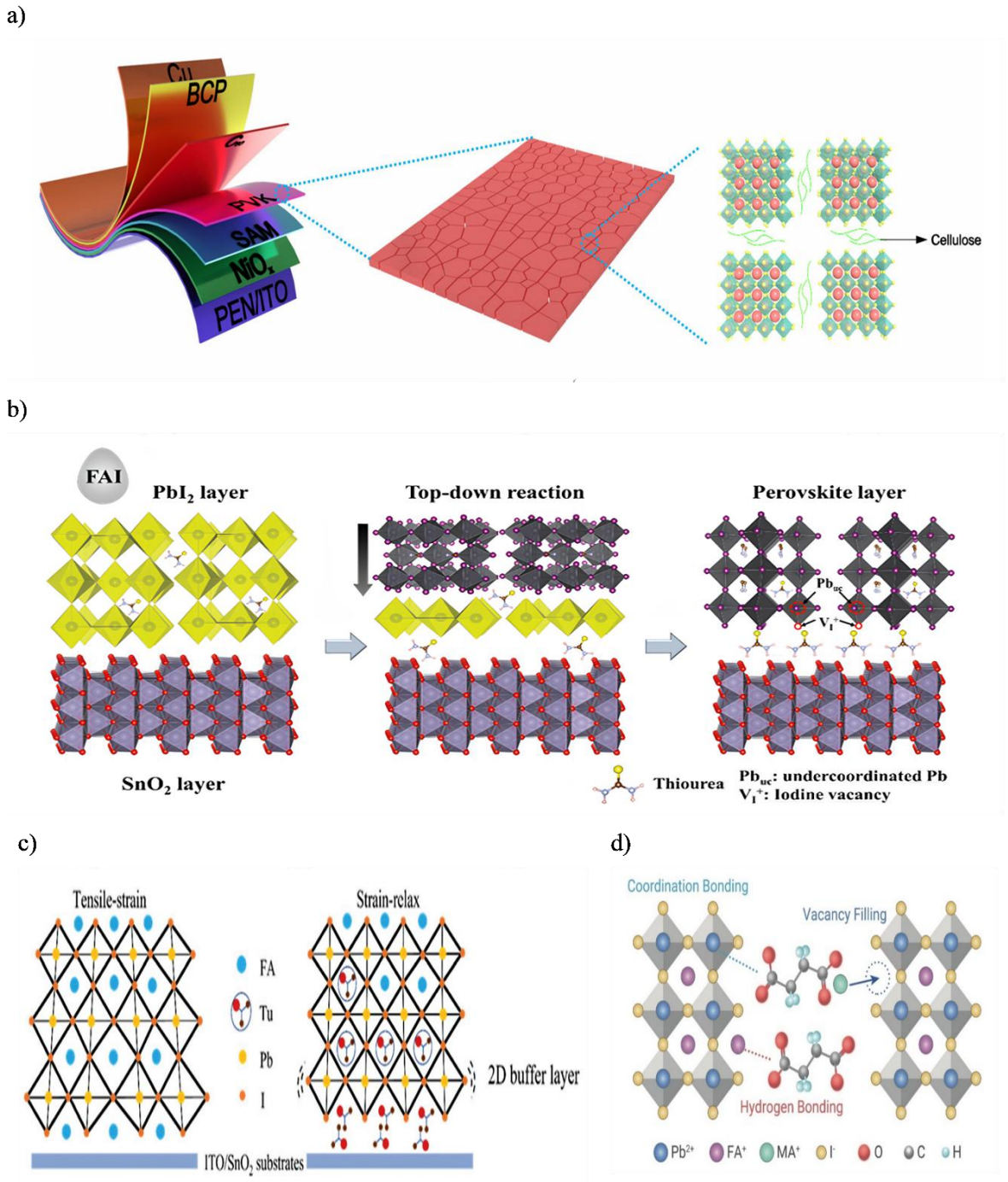

Figure 4. (**a**) Schematic diagram of flexible p–i–n structure solar cells and interaction mechanism between cellulose diacetate and perovskite. Reproduced with permission [36]. Copyright 2025, Solar RRL (**b**) The scheme for the Tu-embedding perovskite crystallization. (**c**) Schematic illustration of the 2D Tu perovskite buffer layer to release the stress. Reproduced with permission [37]. Copyright 2022, Adv. Functional (**d**) Proposed mechanism of the bilateral MS molecule at the perovskite grain boundaries. Reproduced with permission [38]. Copyright 2022, The innovation.

2.5. Band Additives to Guide Crystalline Orientation

The solution process is currently the technology that is most frequently used for creating perovskite films which include one-step and two-step deposition techniques. However, these solution-processed perovskite films confront complicated crystallization and growth processes, which will produce different crystal orientations and morphologies, that can result in variations in device performance. Most importantly, owing to the anisotropy of perovskite crystals, the photoelectric properties may vary with crystal orientation. The irregular crystal orientation of the solution-processed perovskite film exacerbates charge recombination and ion migration within the devices, limiting their stability and power conversion efficiency (PCE) [39,40]. Perovskite films with preferred orientation are requisite for better charge transport, giving rise to higher J_{SC} and FF. Different approaches for improving oriented growth of perovskite films, key factors such as raw materials and solvents for perovskite precursor, annealing temperature, atmosphere, additives, and interfaces. Herein, we summarize various additives for modulating the oriented growth of perovskite films. In this aspect, xu et al. employed nitrogen-doped carbon nanofibers (N-CNFs) via electrospinning technology into the perovskite film to guide the preferential orientation of perovskite crystals Figure 5a [41]. The electrospun N-CNFs possess a high aspect ratio and a surface rich in nitrogen-containing functional groups such as C–N and C=N. These functional groups act as Lewis bases, forming strong coordinate bonds with Pb^{2+} ions from the lead iodide (PbI_2) precursor. This interaction provides a heterogeneous nucleation site as an intermediate phase, guiding grain growth and increasing grain size. Moreover, the fibrous morphology of the N-CNFs imposes a physical constraint that directs the growth of perovskite crystals along a preferential orientation. Secondly, N-CNFs can coordinate with lead ions and lower the trap states brought on by inadequate lead ion coordination, which impedes ion migration. Grazing-incidence wide-angle X-ray scattering (GIWAXS) analysis confirms an enhanced preferential orientation in the (110) plane for films incorporating N-CNFs, evidenced by a strengthened scattering intensity at a 90° azimuth angle Figure 5b. The combined effect of physical templating and chemical passivation promotes a highly crystalline, densely packed, and preferentially oriented perovskite film, which enhances charge carrier transport, improves photovoltaic performance, and significantly boosts the environmental stability of the resulting solar cells. The perovskite solar cell achieved a PCE of 24.08% after doping with N-CNFs.

Generally, the reason perovskite fails to grow into the homogenous and high-crystalline film is due to the multiple pathways of crystal nucleation originating from various intermediate phases in the film-forming process. Li et al. developed a multifunctional fluorinated additive FTPA that effectively restrained the complicated intermediate phase and slowed perovskite crystallization kinetics, allowing for oriented growth of -$FAPbI_3$ Figure 5c [42]. the strong hydrogen-bonding interactions between the fluorine and oxygen atoms on FTPA and the formamidinium (FA^+) cations in the perovskite precursor. This interaction forms a stable FTPA-FA^+-PbI_2 complex that effectively suppresses the formation of competing intermediate phases—specifically $MA_2Pb_3I_8{\cdot}2DMSO$ and δ-$FAPbI_3$—which typically lead to multiple, disordered nucleation pathways during film formation. By restraining these heterogeneous intermediates, FTPA simplifies the crystallization process into a single, dominant pathway favoring the oriented α-phase of $FAPbI_3$. Furthermore, the polymerization of FTPA occurs concurrently with perovskite crystallization at 100 °C, slowing down the release of ions and increasing the energy barrier for nucleation. This retarded crystallization kinetics promotes the growth of larger, highly oriented grains with reduced defects and minimized lattice strain. Due to several improvements, including balanced charge transport, low defect density, and gradient energy-level alignment, the corresponding PSCs demonstrated excellent PCE up to 24.10%. Furthermore, the stabilized -$FAPbI_3$ imparted the PSCs with excellent illumination, moisture, and thermal stability due to the formation of the hydrogen-bonding polymer network in the perovskite film. Wu et al. introduced a new ammonium salt of 2-amidinopyrimidine hydrochloride (APC) additive into the $FAPbI_3$ wet perovskite film for modulating both the crystallization and the charged traps at the same time [43]. Specifically, APC contains functional groups such as pyrimidine nitrogen atoms, amino groups, and chloride ions, which collectively influence the crystallization process by modulating nucleation and crystal growth dynamics. APC interacts with lead iodide (PbI_2) and formamidinium iodide (FAI) precursors through Lewis acid-base coordination and hydrogen bonding. The pyrimidine nitrogen atoms donate lone pair electrons to under-coordinated Pb^{2+} ions, stabilizing the perovskite lattice and reducing the formation of iodine vacancies. Simultaneously, the amino groups and chloride ions form hydrogen or ionic bonds with iodide ions, compensating for FA^+ vacancies and further promoting a more ordered crystal structure Figure 5d. These interactions lower the energy barrier for nucleation and favor crystal growth along the (100) plane. The chloride ions in APC play a particularly important role in passivating interfacial defects and directing oriented crystal growth, leading to larger grain sizes and improved crystallinity. This synergistic regulation of crystallization by APC results in a highly oriented, low-defect perovskite film with enhanced optoelectronic properties. As a result, $FAPbI_3$ planar perovskite film exhibited a PCE of 25.17%.

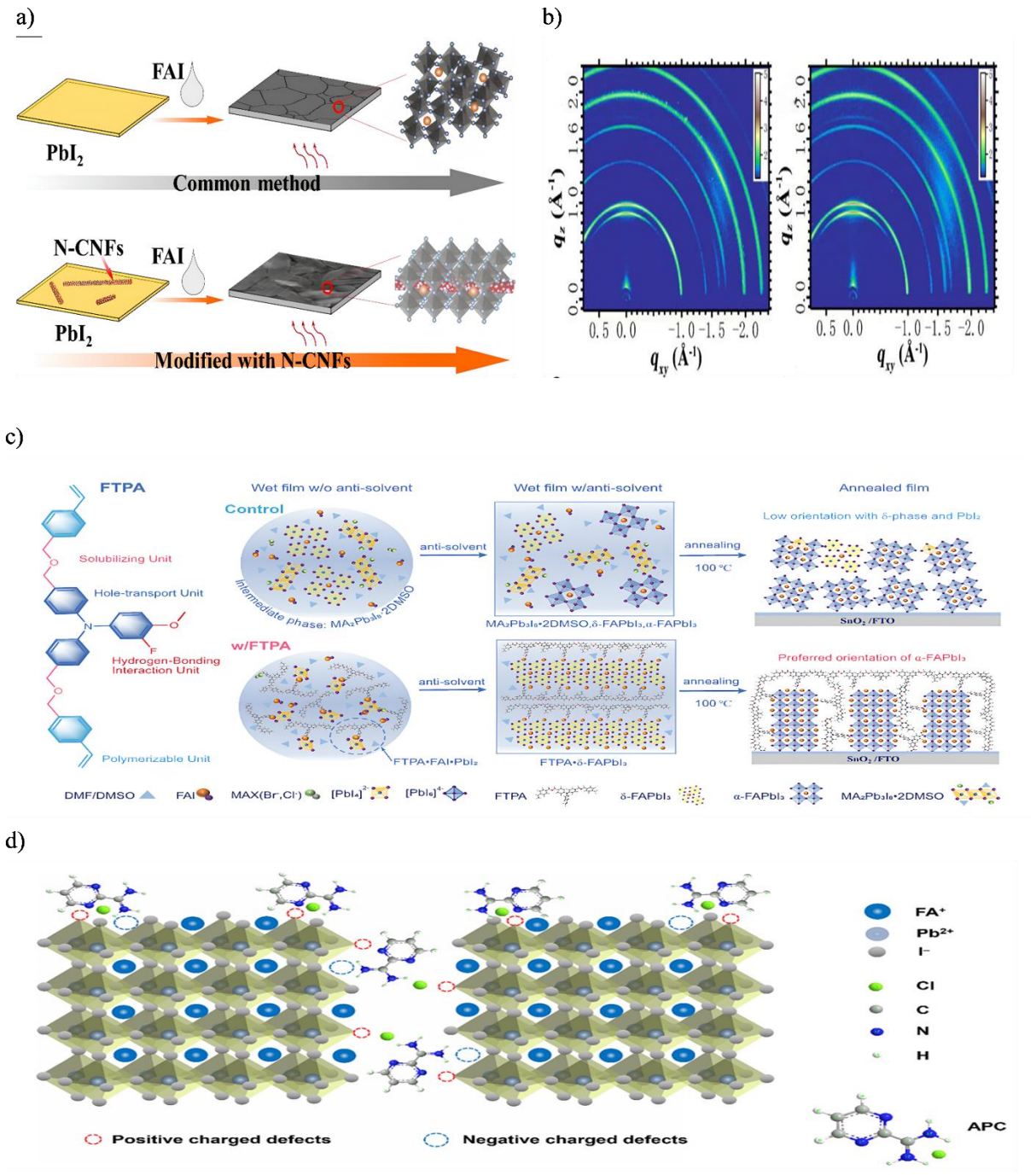

Figure 5. (**a**) N-CNFs application in perovskite solar cells. (**b**) 2D GIWAXS patterns from perovskite films (**a**) without, (**b**) with 0.2 mg·mL^{-1} N-CNFs. Reproduced with permission [41]. Copyright 2022, Chemical Engineering Journal (**c**) Molecular structure design of FTPA, and schematic diagram of the possible phase evolution of the nucleation and crystallization of FA-based mixed anion perovskites ($FA_{0.95}MA_{0.05}Pb(I_{0.95}Br_{0.05})_3$) during the film-forming process with (w) or without (w/o) FTPA. Reproduced with permission [42]. Copyright 2023, Nature Communications (**d**) Schematic illustration of the proposed interaction mechanism between APC and the perovskite. Reproduced with permission [43]. Copyright 2022, Energy Environmental science.

Table 1. Performance summary of FA based perovskite solar cells with the respective additives.

Deposition Film	Additive	Primary Mechanism of Action	PCE (%)	V_{oc} (V)	J_{sc} (mA cm^{-2})	FF (%)
	MACl and $PbCl_2$ [26]	Phase stabilization	26.17	1.187	26.17	84.24
	MEA and CsI [31]	Manage excess PbI_2	25.66	1.199	25.56	83.70
	RbCl [30]	Manage excess PbI_2	25.64	1.16	26.16	84.28
	Methylammonium succinate [38]	Stress relief	25.40	1.164	26.31	82.82
	DFA [23]	Retard crystallization	25.28	1.128	25.62	77.89

Table 1. *Cont.*

Deposition Film	Additive	Primary Mechanism of Action	PCE (%)	V_{oc} (V)	J_{sc} (mA cm^{-2})	FF (%)
FA-based perovskite	$(MDACl_2)$ + (CsI) [44]	Stress relief	25.17	1.168	26.23	82.15
	2-amidinopyrimidine hydrochloride [43]	Organize orientation	25.17	1.184	25.30	84.04
	C-Im-CN [32]	Manage excess PbI_2	24.71	1.20	25.69	80.45
	Cellulose diacetate (CDA) [36]	Stress relief	24.68	1.182	24.81	84.16
	phenyltrimethylammonium chloride (PTAC) [25]	Phase stabilization	24.51	1.182	25.24	82.15
	Thiourea [37]	Stress relief	24.42	1.18	25.70	80.33
	$(NpMA)_2PbI_4$ seed [45]	Organize orientation	24.37	1.18	25.30	81.36
	CdI_2 [46]	Manage excess PbI_2	24.26	1.18	25.2	81.58
	3-Guanidinopropionicacid [47]	Manage excess PbI_2	24.2	1.17	25.27	81.68
	Fluorinated molecule FTPA [42]	Organize orientation	24.10	1.182	24.43	83.45
	N-CNFs [41]	Organize orientation	24.08	1.16	25.53	81.52
	Lanz [24]	Retard crystallization	24.05	1.153	25.27	82.50

3. Additive in other Perovskite Materials

3.1. Additives in MA-Based Perovskite

The $MAPbI_3$ often demonstrates advantages over $FAPbI_3$ in terms of phase stability at room temperature, ease of fabrication, hysteresis, and defect tolerance, making it more reliable for lab-scale and some commercial applications. Additives have similarly greatly improved crystallinity in MA-based perovskite [48]. Liu et al. used antimony acetate (Sb $(Ac)_3$) to enhance the photovoltaic performance of $MAPbI_3$-based PSCs by improving the film quality and optimizing the photoelectronic properties of halide perovskites [49]. Ac^- acts as a crystal growth regulator via forming strong hydrogen bonding between MA^+ and O in Sb $(Ac)_3$ and this forms intermediate complex that slow down crystallization, allowing for more ordered and larger grain growth while Sb^{3+} acts as an electronic optimizer as it is more effective in tuning the energy levels of perovskite films. Sb^{3+} incorporates into the perovskite lattice, likely as an interstitial dopant. Its 5p orbitals hybridize with the I 5p and Pb 6p states, pushing the conduction band to higher energy for better charge extraction. XRD technique was used to analyse the influence of Sb $(Ac)_3$ additive on the crystallinity and the crystal structure of $MAPbI_3$ perovskite film. The main characteristic peaks appeared at 2θ of 14.29°, 28.38° in all samples, corresponding to the (110) and (220) crystal planes of the tetragonal perovskite structure, respectively Figure 6a. This confirms the successful formation of the perovskite phase in all samples. It was found that the (110) and (220) diffraction peaks Figure 6b gradually shifted to a smaller angle with the increased amount of $Sb(Ac)_3$ additive, meaning the expanded crystal lattice induced by Ac^- or Sb^{3+} doping. With the assistance of $Sb(Ac)_3$, the modified $MAPbI_3$-based device delivered a high PCE of 21.04% and exhibited decent stability. In another case Shi et al. adopted a bifunctional additive biuret compound with multiple Lewis base sites (C=O and N-H groups), which acts as an oxygen donor Lewis base coordinates with the Lewis acid PbI_2 in the precursor solution to retard the perovskite crystallization process by forming a stable intermediate adduct MAI-PbI_2-DMSO-biuret between biuret and PbI_2 [50]. The resulting Lewis acid-base adduct in the precursor solution can raise the solubility of lead halides, contributing to the formation of a more uniform intermediate phase and, consequently, a more homogeneous perovskite film [51–53]. The residual biuret efficiently passivates charged ionic defects. Meanwhile, the thermal durability of the $MAPbI_3$ film is enhanced due to the crosslink of biuret and PbI_2 through hydrogen bonds via its N-H groups. This creates a robust chemical bridge between grains, strengthening the microstructure. This crosslinking increases the activation energy for thermal decomposition, making it much harder for the organic MA^+ cation to escape (which is the first step of degradation into PbI_2). The biuret produces high-quality $MAPbI_3$ perovskite film with lower grain boundaries due to large crystal size and defects passivation Figure 6c. The XRD patterns reveal no additional peaks or peak shifts after the addition of biuret, indicating that the biuret additive enhances the crystallinity and grain size of the perovskite film without altering its fundamental crystal structure Figure 6d. With an optimal biuret additive of 2 mol%, the PCE is significantly increased from 18.26% for the reference $MAPbI_3$ solar cell to 21.16% which is among the highest efficiency for $MAPbI_3$ solar cells with the mesoscopic structure. Zhu et al. used cost effective and renewable biomass based two ecofriendly hydroxyalkyl cellulose additives, i.e., hydroxyethyl cellulose (HEC) and hydroxylpropyl cellulose (HPC) in $MAPbl_3$ based inverted PSC Figure 6e [54]. Due to the strong interaction between the hydroxyl groups (-OH) of cellulose and the divalent Pb^{2+} cations in the perovskite creates a transient HEC-PbI_2 or HPC-PbI_2 complex. This complex acts as a scaffold or a template around which the perovskite

crystals must form. This complex slows ion diffusion and crystallization. Consequently, these additives improve crystal grain alignment and effectively heal defects in the perovskite films. Acting as passivation agents, the two cellulose derivatives demonstrate a remarkable ability to reduce trap states, thereby enhancing the optoelectronic properties of perovskite solar cells (PSCs). The power conversion efficiency (PCE) shows a significant improvement, increasing from 19.21% for the additive-free device to 20.45% with HPC and further to 21.25% with HEC. Tao et al. employed methylamine cyanate (MAOCN) molecules in $MAPbI_3$ solutions to manipulate the crystallization of the $MAPbI_3$ films [55]. MAOCN molecules can slow down the solvent's volatilization rate and delay the crystallization process of the $MAPbI_3$ film by forming intermediate complexes such as CH_3NH_3I–NMP–PbI_2, which helps to increase the grain size and suppress the defect formation Figure 6f. MAOCN decomposes during annealing into volatile products (HOCN and CH_3NH_2), which evaporate along with residual solvents, leaving no harmful residues. The $MAPbI_3$ film based on MAOCN has a more hydrophobic surface, a longer carrier lifetime, and increasing moisture stability. The efficiency of $MAPbI_3$- film based on MAOCN reached 21.28%. A comparative summary of the performance metrics for MA-based PSCs employing different additives is presented in Table 2.

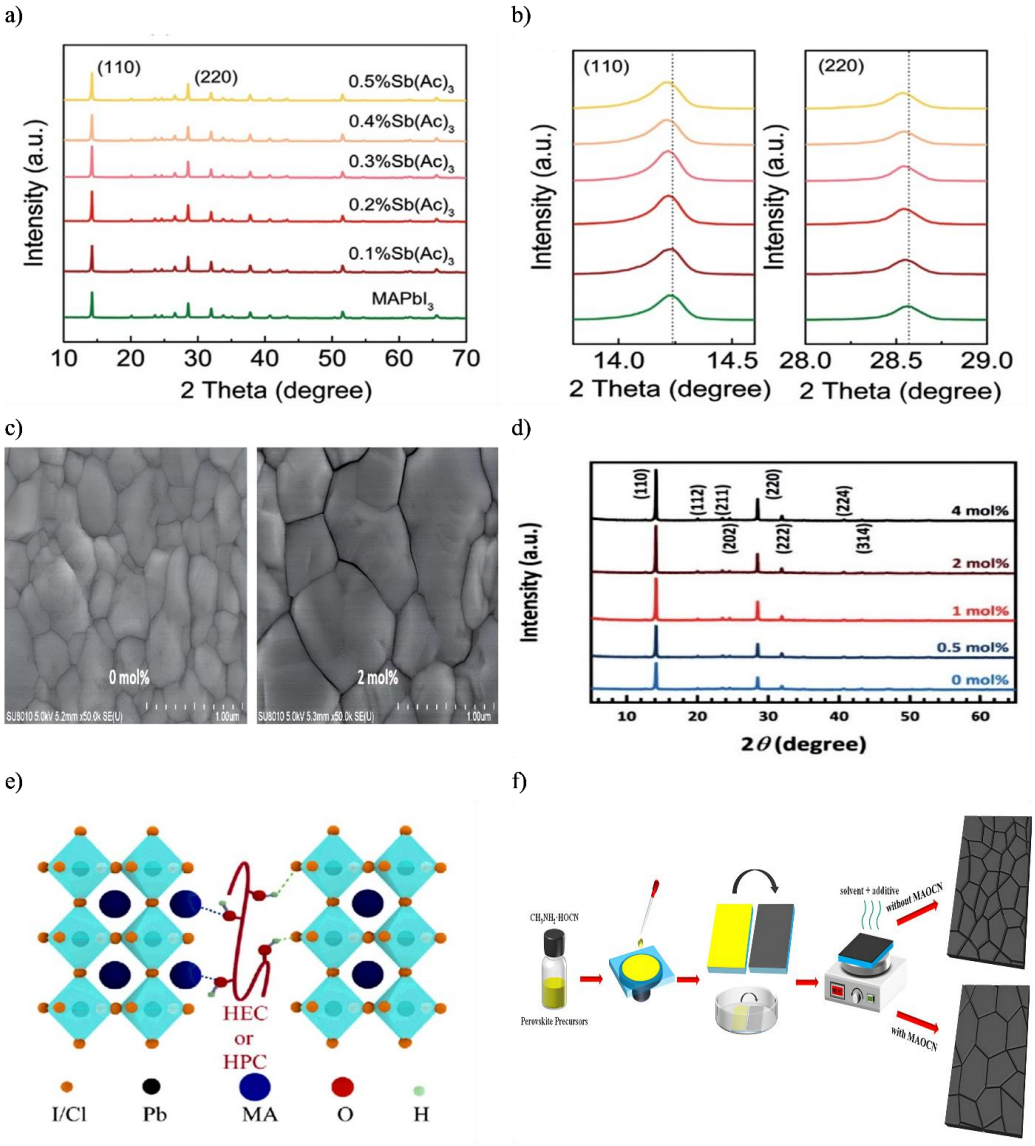

Figure 6. (**a**) XRD of $MAPbI_3$ perovskite films without and with different amounts of $Sb(Ac)_3$ additive. (**b**) relevant enlarged (110) and (220) diffraction peaks of $MAPbI_3$ perovskite films without and with different amounts of $Sb(Ac)_3$ additive. Reproduced with permission [49]. Copyright 2021, Wiley-VCH GmbH (**c**) SEM images of perovskite films with and without the biuret additive. (**d**) XRD patterns of perovskite films with and without the biuret additive. Reproduced with permission [50]. Copyright 2020, The Royal Society of Chemistry (**e**) Schematic diagram for the interaction of HEC/HPC and perovskite. Reproduced with permission [54]. Copyright 2022, Energy & Environmental materials (**f**) Schematic diagram of the preparation process of perovskite films with and without MAOCN. Reproduced with permission [55]. Copyright 2021, ACS Appl. Mater. Interfaces.

Table 2. Performance summary of MA based perovskite solar cells with the respective additives.

Deposition Film	Additive	Primary Mechanism of Action	PCE (%)	V_{oc} (V)	J_{sc} (mA cm^{-2})	FF (%)
MA-based perovskite	methylamine cyanate (MAOCN) [55]	Retard crystallization	21.28	1.12	23.29	81.13
	HEC [54]	Organize orientation	21.25	1.16	22.98	79.71
	Biuret [50]	Retard crystallization	21.16	1.11	23.55	80.73
	Antimony acetate $Sb(Ac)_3$ [49]	crystal growth regulator	21.04	1.1	24.19	79.1
	HPC [54]	Organize orientation	20.45	1.15	22.44	78.82
	Ammonium Benzenesulfonate ABS [56]	Retard crystallization	20.62	1.12	23.53	78.54
	Ethyammonium chloride EACL [57]	Retard crystallization	20.03	1.08	23.51	76.99

3.2. Additives in All Inorganic Perovskite

The Organic-inorganic hybrid perovskites suffer from chemical instability when exposed to oxygen, moisture, light, and, notably, high temperatures, due to organic cations' hygroscopic and volatile character. It is commonly known that inorganic materials are more stable at high temperatures than organic materials [58–60]. The inorganic monovalent cation Cs^+, which may replace MA^+ and FA^+ as the A-site ions to generate high thermally stable $CsBX_3$ perovskites (>350 °C), has been found to meet the criteria of the ABX_3 structure. At the same time, due to its excellent broad bandgap, $CsBX_3$ perovskite is the ideal candidate for tandem solar cell fabrication. One of the main challenges in achieving high photovoltaic performance for $CsPbX_3$ is the fabrication of a highly crystalline perovskite film with a uniform surface, a large grain size, and a low defect density. Unfortunately, due to the relatively quick crystallization, the defect sites that would be the recombination centre are inevitably formed in most solution-processed $CsPbX_3$ films [61–63]. In this regard, Peng and coworkers used a non-ionic additive of polyethyleneimine (PEI) with multiple amino groups (–NH_2 and –NH–) act as Lewis bases in a $CsPbI_2Br$ film to develop hydrogen bonds with I-/Br- ions reducing halide vacancy defects and coordinate with Pb^{+2}/Cs^+ ions reducing metal vacancy defects [64]. The long alkyl chain of PEI regulates crystal growth. The physical presence of the long polymer chain adsorbed on the crystal surface creates a physical barrier. It sterically hinders the approach and attachment of new ions to the growing crystal lattice, effectively slowing down the growth rate. The strong interaction between PEI and $CsPbI_2Br$ yields a well-controlled grain size, fewer defects, and a reinforced phase structure of $CsPbI_2Br$ film, increasing the power conversion efficiency (PCE) of perovskite solar cells to 15.48% Figure 7a. The negligible difference of the XRD spectrum between $CsPbI_2Br$ and $CsPbI_2Br$–PEI films indicates that the crystal structures are not affected by the amplification of PEI Figure 7b. Lü et al. introduced dicyandiamide (DCD) as a Lewis base additive to enhance the efficiency and stability of $CsPbIxBr_{3-x}$ (x = 2.65) of carbon-based inorganic perovskite C-PSCs [65]. The $CsPbI_xBr_{3-x}$ perovskite in this study is formed using a DMAI (Dimethylammonium Iodide)-assisted method. This process involves an intermediate phase, $DMAPbI_3$, which must decompose so that volatile DMA^+ can escape and be replaced by Cs^+ to form the final inorganic perovskite. Unlike additives that slow down crystallization, DCD accelerates this specific phase transition. DCD promotes the rapid decomposition of the $DMAPbI_3$ intermediate and facilitates the complete ion exchange between DMA^+ and Cs^+. This results in a more complete and purer perovskite phase with no residual organic intermediate, which is crucial for high thermal stability. The lattice constant also contracts, confirming the successful replacement of larger DMA^+ with smaller Cs^+ ions. This in-situ XRD study (Figure 7c) revealed the primary mechanism of DCD's action on crystallization kinetics. In the control film, a strong persistent signal was observed from the $DMAPbI_3$ intermediate phase (at ~11.6°) even after 20 min of annealing. This indicates an incomplete and slow transition to the final perovskite phase. In contrast, the DCD-modified film shows a rapid and complete consumption of the $DMAPbI_3$ intermediate. The perovskite phase forms quickly and dominates. DCD's cyano (C≡N) and imine (C=N) groups passivate defects by coordinating with uncoordinated Pb^{2+}, yielding high-quality perovskite films with enlarged grains and improved crystallinity. The optimized energy level alignment boosts the PCE from 14.07% to 15.84%. Additionally, DCD enhances the film's hydrophobicity, shielding it from moisture and improving air stability, while the complete volatilization of dimethylamine (DMA^+) strengthens thermal stability. Fu et al. revealed that introducing a novel multifunctional liquid additive, 2-hydroxyethyl methacrylate (HEMA), into the $CsPbI_2Br$ precursor can ameliorate issues of unsatisfactory crystallization quality and moisture instability [66]. HEMA molecules in perovskite film will polymerize to a hydrophobic polymer at GBs through

breaking C = C bonds, moreover, it effectively connects the neighbouring perovskite grain and boosts the tolerance to moisture, thus blocking moisture penetration. Importantly, HEMA with functional groups of C = O act as an active site to coordinate effectively with Pb^{2+} ions and -OH interact with I^- and Br^- anions via hydrogen bonding. This interaction slows down the crystallization kinetics by temporarily "capping" the precursor ions. This allows for a more controlled and ordered crystal growth results in increased grain size (from 0.55 μm to 0.85 μm), reduce grain boundaries, smooth film surface Figure 7d,e. HEMA additive leads to a champion power conversion efficiency of up to 16.13%. During the high-temperature annealing process (160 °C), the vinyl group (C=C) in HEMA breaks and undergoes polymerization. The small, hydrophilic HEMA molecules transform into a hydrophobic polymer (poly-HEMA) that resides at the grain boundaries. The polymer crosslinks and encapsulates the perovskite grains. It physically blocks pathways for water vapor to penetrate and degrade the film. Thus, the unencapsulated device maintains 78% of its initial efficiency after aging at 30% relative humidity for 1000 h. Table 3 benchmarks the performance of all inorganic PSCs using various additives.

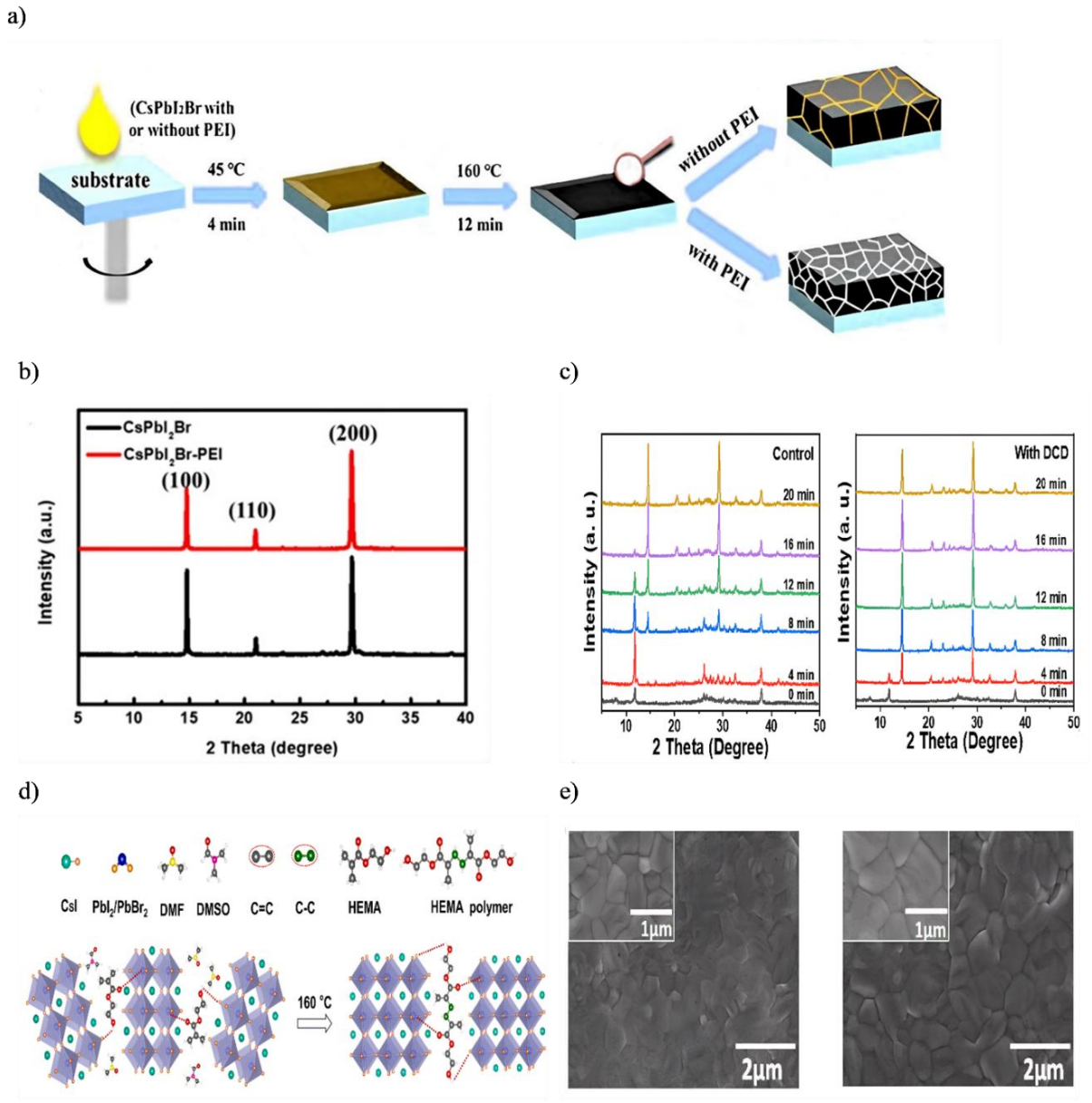

Figure 7. (**a**) Schematic diagram of $CsPbI_2Br$ with and without PEI thin-film preparation process and difference of grain growth. (**b**) XRD spectra of the $CsPbI_2Br$ and $CsPbI_2Br$-PEI thin films. Reproduced with permission [64]. Copyright 2020, Solar RRL (**c**) XRD patterns of the control CsPbIxBr3-x film and with DCD at different annealing time. Reproduced with permission [65]. Copyright 2024, Materials Today Energy (**d**) Schematic representation of the presence of HEMA hydrophobic polymers at GBs (**e**) Top-view SEM images of the perovskite films w/o and with HEMA. Reproduced with permission [66]. Copyright 2021, Chemical Engineering Journal.

Table 3. Performance summary of all inorganic based perovskite solar cells with the respective additives.

Deposition Film	Additive	Primary Mechanism of Action	PCE (%)	V_{oc} (V)	J_{sc} (mA cm^{-2})	FF (%)
all-inorganic perovskite	2-hydroxyethyl methacrylate [66]	Grain boundary encapsulation	16.13	1.23	15.81	82.98
	dicyandiamide DCD [65]	Retard crystallization	15.84	1.14	17.82	77.91
	polyethyleneimine (PEI) [64]	Retard crystallization	15.48	1.22	15.56	81
	formamidinium chloride (FACl) [67]	Retard crystallization	15.03	1.28	15.14	77.51

3.3. Additive in Sn-Based Perovskite

Due to the toxicity of lead in Pb-PSCs, their mass production and practical applications may be confined. As a result, developing less toxic or nontoxic lead-free perovskite materials with favourable optoelectronic properties is crucial. As yet, lead-free perovskites based on tin (Sn), bismuth (Bi), antimony (Sb), germanium (Ge), titanium (Ti), and copper (Cu) have been researched. Sn, which has a similar outer electronic configuration (ns2 np2) and ionic radius to Pb, can be used to completely replace the lead element in perovskite crystals without causing significant lattice distortion or phase segregation, which is the most promising of these alternatives. Furthermore, tin perovskite has an ideal optical bandgap near the Shockley-Queisser limit (1.3–1.4 eV), a low exciton binding energy, and high charge-carrier mobility. Sn-perovskites appear to be the most promising alternatives, and many efforts have been made in recent years to develop Sn-PSCs [68–70]. Until now, the highest PCE reported for Sn-PSCs is significantly lower than the state-of-the-art Pb-PSCs. The oxidative instability of Sn^{2+}, which easily results in high defect density in perovskite films, is one of the major challenges. The other issue is the rapid crystallization of Sn-perovskites, which severely impedes film coverage, crystallinity, and reproducibility. Therefore, controlling crystallization is in fact equally important to achieve good device performance. To address this, Li et al. reported a novel cation exchange strategy (CES) for producing high-quality formamidinium tin iodide ($FASnI_3$) perovskite films with improved crystallization process control and reproducibility [71]. Formamidine acetate salt (FAAc) and methylammonium iodide (MAI) are used as dual cation sources in a perovskite precursor solution instead of the typically used formamidinium iodide (FAI), which would result in the formation of mixed organic-cation $MA_xFA_{1-x}SnI_3$ perovskites after film deposition. Upon thermal annealing, the free FA^+ from FAAc would replace the MA^+ in the perovskite lattice, accompanied by the volatilization of MAAc, leaving pure $FASnI_3$ perovskite films. The cation exchange process, instead of FAs directly entering, successfully slowed down the crystal growth rate, plus the existence of Lewis base Ac^- would reduce the crystallization rate of the Sn-perovskite which effectively improves the perovskite quality with oriented crystal growth, enlarged grain size, and lower defect density Figure 8a. The corresponding Sn-PSCs exhibit excellent photovoltaic performance, with a champion efficiency of 9.11%, comparable to the best $FASnI_3$-PSC results reported. Li et al. incorporated the ionic liquid *n*-butylammonium acetate (BAAc) to modulate precursor coordination and crystallization, yielding high-quality perovskite films. BAAc forms solid O…Sn chelating bonds and N-H…X hydrogen bonds with the precursors, slowing crystal growth and enabling uniform nucleation, thus producing pinhole-free, preferentially oriented films Figure 8b. XRD analysis revealed intensified (100) and (200) diffraction peaks at 14.7° and 28.8° Figure 8c, confirming enhanced crystallinity. This preferred orientation improves vertical charge transport, leading to a record PCE of 10.4% in inverted *p-i-n* planar devices. Su et al. introduced acetic acid (HAc) which acts as a multi-functional additive in tin-based perovskite solar cells by simultaneously regulating crystallization kinetics and suppressing Sn^{2+} oxidation. It reduces the supersaturation concentration of the precursor solution, promoting the formation of pre-nucleation clusters that lower the nucleation energy barrier and enable rapid, uniform nucleation. This leads to dense, pinhole-free films with larger grains and reduced tensile strain. At the same time, HAc partially ionizes in the precursor to create a weakly acidic environment in which Sn^{2+} remains thermodynamically stable, thereby inhibiting its oxidation to Sn^{4+}, while the acetate ion passivates uncoordinated Sn defects. In addition, the hydroxyl group (O–H) of HAc forms hydrogen bonds with iodide ions, immobilizing them and preventing volatilization. This helps preserve the I^-/Sn^{2+} stoichiometric ratio near the ideal 3:1 value, reducing vacancy defects and minimizing lattice distortion Figure 8d. The HAc-modified Sn-based PVSCs achieved a record PCE of 12.26% with superior open-circuit voltage up to 0.75 V. Moreover, the unencapsulated device maintains nearly 90% of the initial PCE even after 3000 h storage in nitrogen atmosphere. Tang et al. used $ZnAc_2$ to stabilize the $FAI{\cdot}SnI_2$ intermediate phase in $FASnI_3$, slowing crystallization and preventing Sn^{2+} oxidation [72]. Zn^{2+} also improved nucleation, yielding larger grains. The $ZnAc_2$-$SnCl_2$ complex further protected the film, increasing PCE from 6.70% to 8.38%.

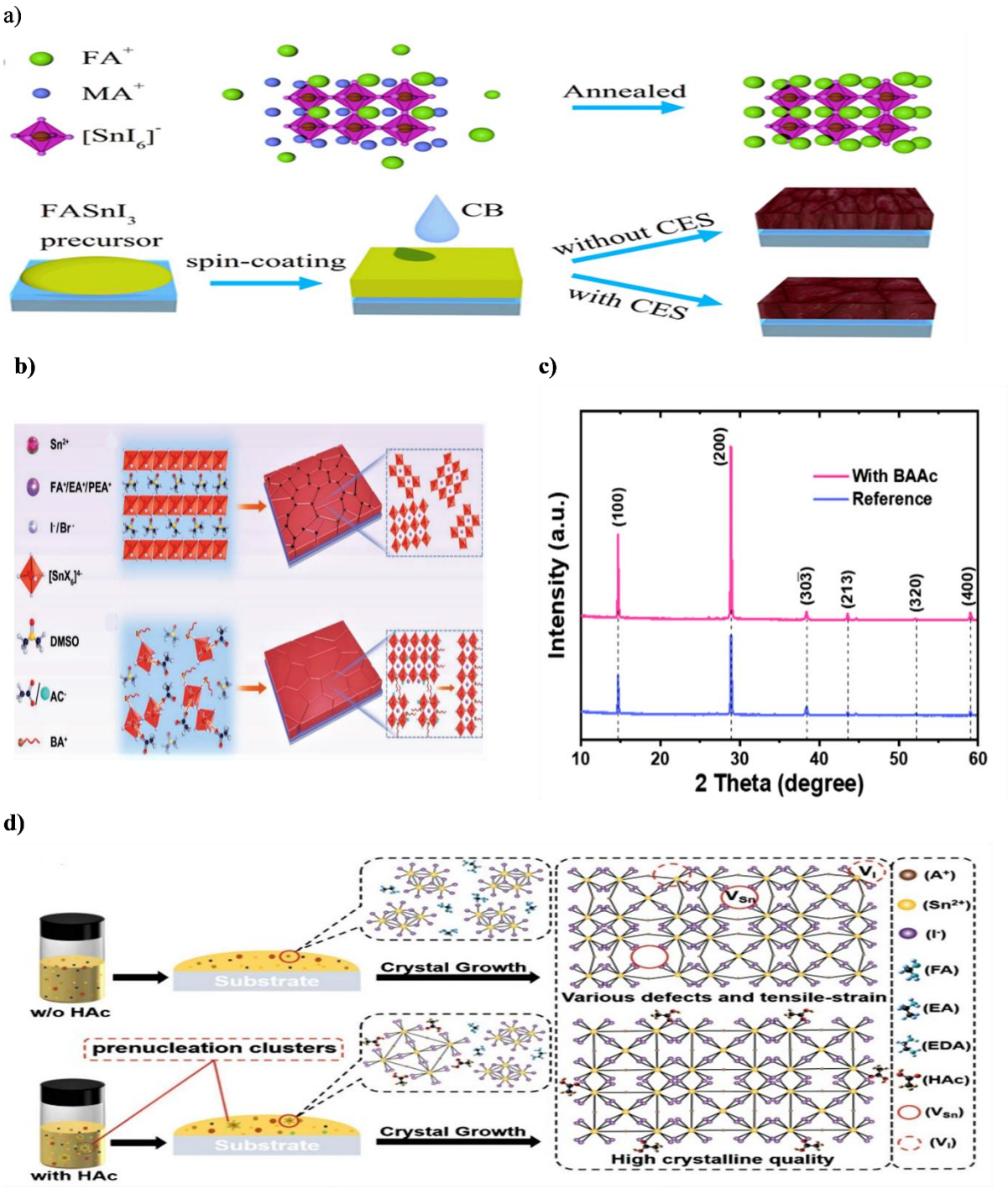

Figure 8. (**a**) Schematic diagram of Cation exchange strategy. Reproduced with permission [71]. Copyright 2021, ACS Appl. Mater. interfaces (**b**) Schematic illustration of BAAc ionic liquid-assisted crystallization kinetics of Sn-based perovskite films. Perovskite films processed without and with BAAc. (**c**) XRD patterns of the reference and BAAc-containing films. Reproduced with permission [73]. Copyright 2021, Adv. Energy Materials (**d**) Schematic illustration: the effect of acetic acid (HAc) on regulation of crystallization kinetics and improvement of crystalline quality. Reproduced with permission [74]. Copyright 2022, Adv. Functional Materials.

3.4. Additive in Sb-Based Perovskite

Antimony (Sb) has emerged as a viable replacement for poisonous lead (Pb) in perovskite material [75,76]. However, Antimony (Sb^{3+}) possesses a stereochemical active lone electron pair that accommodate non-octahedral coordination, restrict the formation of a uniform 3D perovskite. This intrinsic tendency causes irregular crystallization, assist low-dimensional structures that grow unevenly and leads to formation in rough, inhomogeneous films with poor morphology. The disorganized growth process also prevents homogeneous halide mixing, bring about segregation and uncontrolled halide constituents throughout the film. Yang et al. proposed

large size LiTFSI with multiple O donors addition strategy into Sb-based perovskite [77]. LiTFSI functions as a crystallization moderator for Sb-based perovskites by temporarily arresting growth and enabling uniform film formation. It first coordinates with $SbCl_3$ to form a stable zero-dimensional MAI–$SbCl_3$–LiTFSI complex, where the bulky LiTFSI induces steric obstacle that prevents uncontrolled direct conversion into two-dimensional structures. This intermediate slows down crystallization, avoiding defects and disordered growth. When the antisolvent (NBA) is introduced, LiTFSI is removed, which triggers uniform heterogeneous nucleation across the substrate. The result is a pinhole-free, highly crystalline two-dimensional film with a stable I/Cl ratio, directly improving morphology and optoelectronic performance Figure 9a,b. Based on this approach, Sb-based perovskite-like solar cells (PLSCs) attain the highest recorded PCE (3.34%) and sustain 90% of the initial PCE after being held at ambient temperature for over 1400 h. Table 4 provides a comparative overview of the performance of Sn and Sb-based PSCs achieved through the use of selected additives.

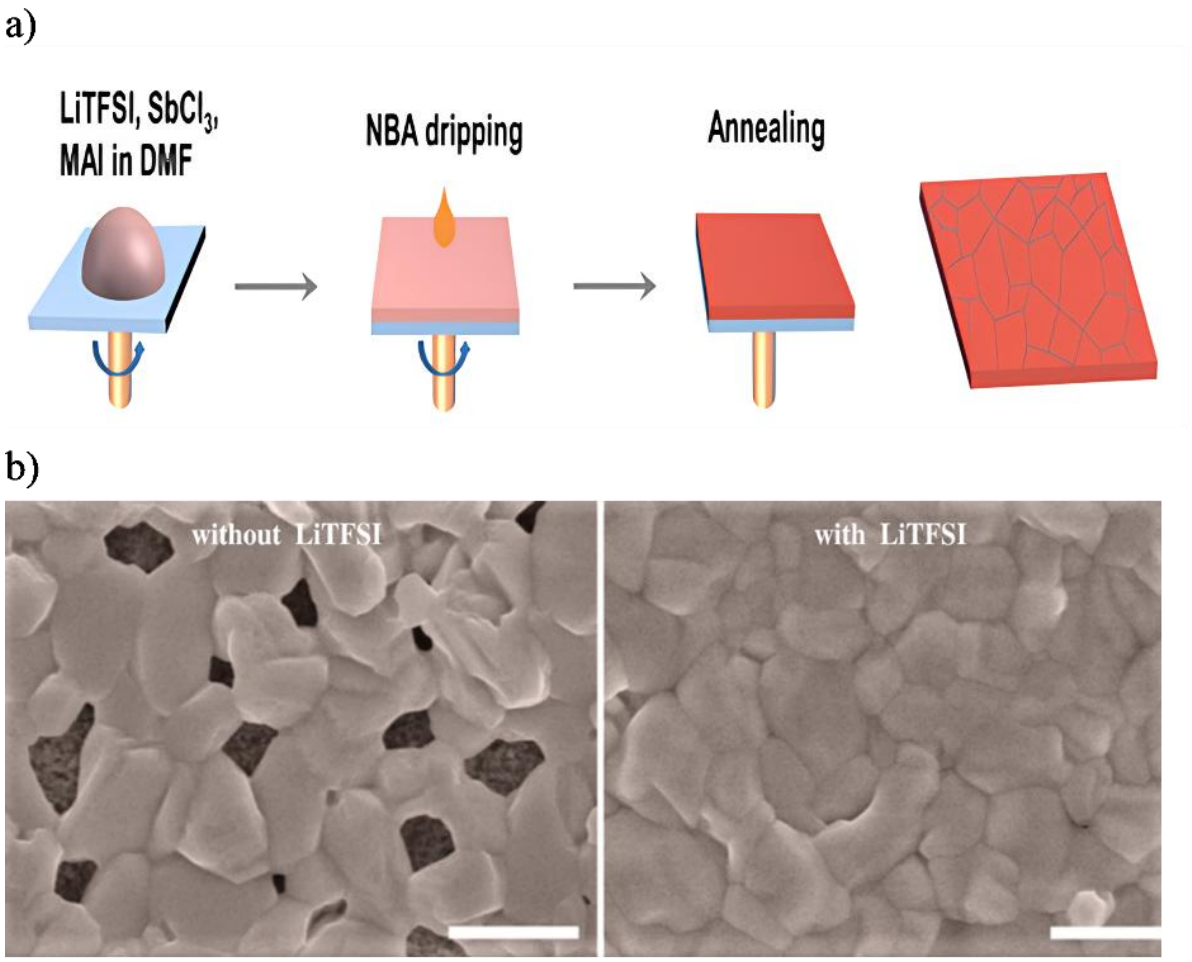

Figure 9. Work (**a**) Schematic of LiTFSI-NBA process used for absorption layer. (**b**) SEM images of the perovskite-like films fabricated by the conventional method (control) and dimension-controlled method (with LiTFSI). Reproduced with permission [77]. Copyright 2020, ACS Appl. Mater. Interfaces.

Table 4. Performance summary of all Sn and Sb based perovskite solar cells with the respective additives.

Deposition Film	Additive	Primary Mechanism of Action	PCE (%)	V_{oc} (V)	J_{sc} (mA cm^{-2})	FF (%)
Sn-based Perovskite	acetic acid (HAc) [74]	Avoid Sn^{2+} oxidation, stress relief	12.26	0.75	21.71	74.97
	n-butylammonium acetate (BAAc) [73]	Retard crystallization	10.4	0.65	22.2	71.6
	Formamidine acetate salt (FAAc), methylammonium iodide (MAI) [71]	Retard crystallization	9.11	0.59	20.54	74.37
	zinc acetate ($ZnAc_2$) [72]	Avoid Sn^{2+} oxidation	8.38	0.54	22.49	69
Sb-based perovskite	bis- LiTFSI) [77]	Organize orientation	3.34	0.70	7.38	65

3.5 Additive in Two-Dimensional Perovskite

In recent years, research on organic-inorganic lead halide two-dimensional (2D) perovskites have been blossoming. The emerging 2D perovskites exhibit superior stability and similar optoelectronic attributes compared to 3D analogous, but their strong exciton-binding energy and inferior interlayer charge-transport reduce dramatically the device performance [78,79]. As bulky organic components were electrically insulating, charge transport would be severely hindered when hopping between the inorganic slabs. In this regard, the orientation of the inorganic perovskite crystals should be a dominating factor in determining the efficiency of PSCs: only vertical stacking provided a direct pathway for efficient charge transport through the perovskite. The growth mechanism of 2D perovskites significantly affects their crystal orientation and, consequently, their photovoltaic performance. Zhang et al. reported an approach towards high-efficiency 2D perovskite solar cells (PSCs) by using the pseudohalides additives, such as methylammonium thiocyanate (MASCN) to control the crystallization mechanism and to rotate the crystallographic orientation of 2D systems [80]. The methylammonium thiocyanate (MASCN), can induce the low-n-value 2D perovskite phases to assemble to a high-n phase distribution. The process is driven by the strong coordination ability of the thiocyanate anion. The SCN^- ion has two potential binding sites: the sulfur (S) and the nitrogen (N) atoms. It can act as a bridging ligand, simultaneously coordinating to the lead (Pb^{2+}) ions on the inorganic framework of multiple perovskite nuclei or small colloidal particles. This bridging action effectively "glues" smaller, low-*n* quantum well fragments together, facilitating their assembly into larger structures with a higher number of inorganic layers (high-*n* phases). Concurrently, the SCN^- ions passivate defects and modulate the crystallization kinetics. By binding to undercoordinated Pb^{2+} ions at the crystal surface and grain boundaries, they reduce the formation energy of larger, more stable crystals and suppress the random nucleation of small, disparate phases. Thereby improving the corresponding phase distribution and guiding the crystal growth of the 2D framework towards vertical out-of-plane orientation, which strongly improves the 2D crystallinity, charge mobility, and carrier lifetime Figure 10a. Correspondingly, the assembly behaviour increases the perovskite films' grain size, which can also result in a decrease in defects and an improvement in the performance and stability of the device. GIWAXS of the perovskite films exhibit strong, sharp, and discrete Bragg spots, suggesting a preferential crystal growth of the (011) plane and superior crystallinity Figure 10b. As a representative, pseudohalide-optimized perovskite solar cells achieve a champion power conversion efficiency (PCE) of 18.72%, among the best PCEs reported for 2D PSCs. Additionally, the corresponding perovskite solar cells show significant improvement in thermal, environmental, light, and operational stability with pseudohalide optimization. Wang et al. revealed that using the synergistic effect of Methylammonium chloride (MACl) and lead chloride ($PbCl_2$) to prepare high-quality quasi-two-dimensional (Q-2D) Ruddlesden–Popper (RP) perovskite films [81]. The Cl^- ions from MACI have a stronger tendency to coordinate with Pb^{2+} than I^- ions do. This leads to the formation of different, and crucially, more stable intermediate phases. So, incorporating MACl additive slows down the crystallization process of Q-2D perovskites, beneficial for the formation of large and uniform grains. However, MACI is highly volatile. During the thermal annealing step, it rapidly decomposes and escapes as gaseous methylamine (MA) and HCl. Introducing $PbCl_2$ additive prevents the rapid volatilization of MACl by forming $MAPbCl_3$ intermediate phase. During the subsequent thermal annealing, this $MAPbCl_3$ phase slowly transforms into the desired iodine-based perovskite via anion exchange (the Cl is replaced by I). The $MAPbCl_3$ disappears after annealing. This process provides a controlled, slow release of the MA^+ and Cl^- species, which allows the MACI to perform its grain-enlarging function without causing pinholes. Cl^- into the perovskite crystals also passivates the trap states. Figure 10c presents top-view SEM images comparing Q-2D perovskite films with and without additives. The additive-free control film displays a smooth and dense morphology but contains surface cracks. On the other hand, the film treated with MACl and $PbCl_2$ binary additives shows a pinhole-free, compact surface with enlarged grain size. The resulting perovskite solar cells exhibit an outstanding efficiency of 18.67% as well as excellent operational stability as compared with the control ones, which is attributed to the enhanced perovskite quality and better hydrophobicity. The photovoltaic performance of 2D based perovskite solar cells incorporating various additives is summarized in Table 5.

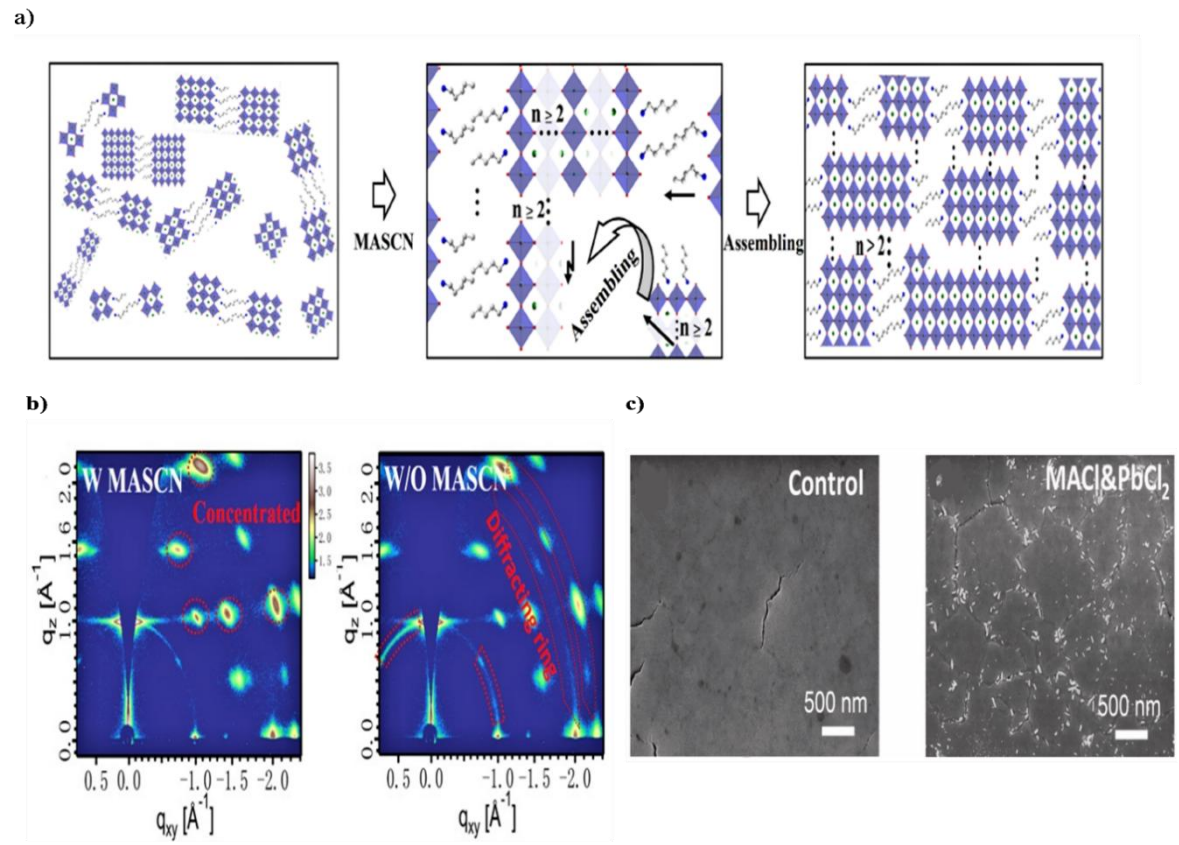

Figure 10. (**a**) Schematic diagram of the assembly behaviour with the addition of the pseudohalide additive. (**b**) GIWAXS images of a pseudohalide optimized 2D perovskite film and reference 2D perovskite. Reproduced with permission [80]. Copyright 2022, ACS Energy Lett (**c**) Top view SEM images of Q-2D perovskite films with and MACl&$PbCl_2$ without binary additives. Reproduced with permission [81]. Copyright 2021, Chemical Engineering Journal.

Table 5. Performance summary of 2D perovskite solar cells with the respective additives.

Deposition Film	Additive	Primary Mechanism of Action	PCE (%)	V_{oc} (V)	J_{sc} (mA cm^{-2})	FF (%)
2D Perovskite	Pseudohalide [80]	Organize orientation	18.72	1.17	20.35	78.03
	MACl&$PbCl_2$ [81]	Retard crystallization	18.67	1.20	18.75	83.0
	NH_4Cl and H_2O [82]	Organize orientation	17.03	1.17	14.49	78.66
	4,5-dicyanoimidazole (DCI) [83]	Phase buffering	17	-	-	-

4. Conclusions and Outlook

This review has demonstrated additive engineering to be a powerful and facile technique for tuning crystal growth and enhancing the photovoltaic performance of different perovskites solar cells (PSCs). The observed improvements in power conversion efficiency (PCE) are primarily attributed to the formation of uniform, high-quality perovskite films with superior optoelectronic properties. The diverse role of additives in addressing the fundamental challenges of perovskite crystallization is conceptually summarized in Figure 11. As illustrated, specific additive classes target distinct challenges—from controlling crystallization kinetics, stabilizing α phase, excess PbI_2, orientation to relieving internal stress and suppressing Sn^{2+} oxidation—resulting in the desired high-quality film with large grains, low defects, and high phase stability.

Despite these noteworthy developments, the path toward commercialization presents several persistent obstacles that must be overcome through future research. Understanding the long-term degradation mechanisms of devices that incorporate additives is a crucial challenge. Future research must concentrate on how these molecular modifiers affect the perovskite lattice in presence of operational stressors such as heat, light, and humidity, as well as whether they unintentionally create new degradation pathways. Currently, most additive-enhanced PSCs remain at Technology Readiness Level TRL 3–4 (lab-scale validation), with a few approaches advancing to TRL 5–6 (prototype testing under realistic conditions). To advance to TRL 7+, future work must focus on long-term outdoor testing, encapsulation standards, and integration with existing PV manufacturing infrastructure.

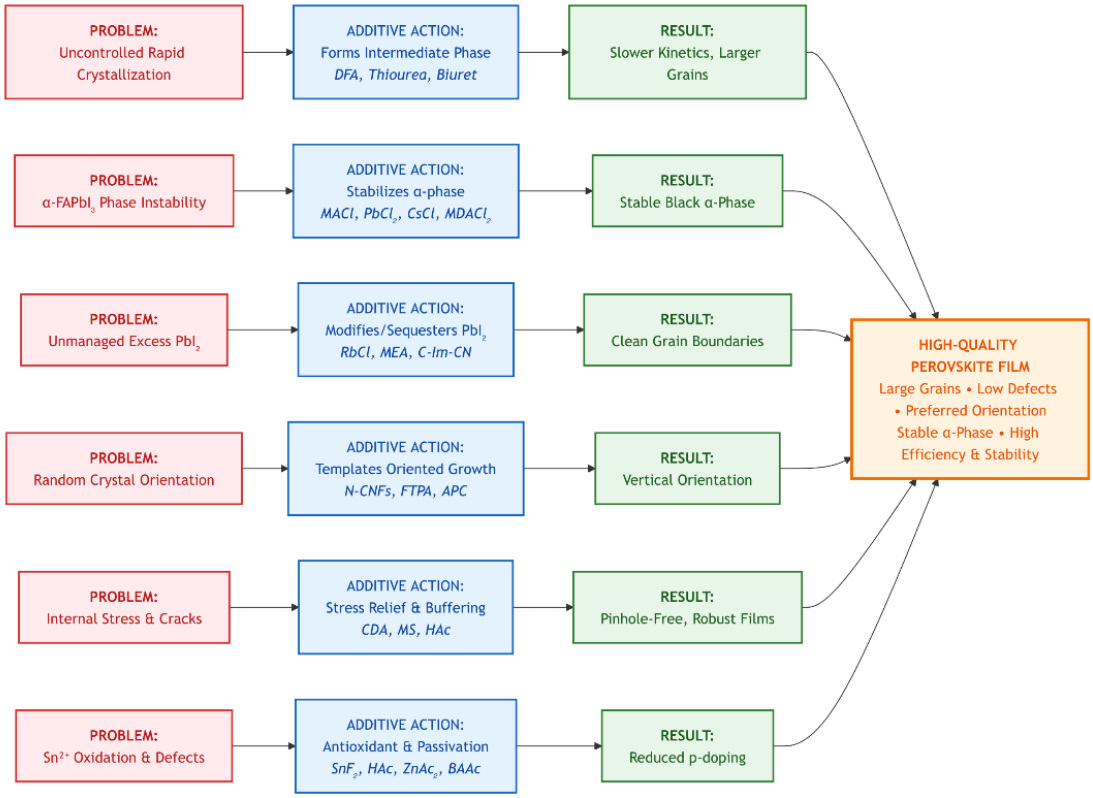

Figure 11. Schematic summary of additive engineering strategies. Different categories of additives target specific crystallization challenges (**top**), through defined mechanisms of action (**center**), to achieve improved film properties and device performance (**below**).

Additionally, while additive engineering has proven highly effective in optimizing perovskite crystallization and film quality at the lab scale—typically via spin-coating—its translation to industrial-scale production needs careful consideration of compatibility with scalable deposition methods such as slot-die coating, blade coating, and inkjet printing. These techniques involve fundamentally different fluid dynamics, drying kinetics, and nucleation environment compared to spin-coating, often leading to challenges in uniform crystallization over large areas. Several studies have begun to explore the role of additives in facilitating scalable fabrication. For instance, polymer additives (e.g., polyethylene oxide, cellulose derivatives) can modulate viscosity and suppress uncontrolled crystallization, enabling smoother ink spreading and better wetting during blade coating. Similarly, volatile additives (e.g., MACl, DMSO) that promote intermediate phase formation can extend the processing window, allowing for better crystal alignment and reduced pinhole formation under slower drying conditions. Recent research by Wang et al. demonstrated that incorporating a small amount of a Lewis base additive into a slot-die-coated perovskite ink considerably improved grain orientation and device reproducibility on mini-module scales. However, there are still significant obstacles. Many functional additives—especially those depend on strong coordination with Pb^{2+} or forming non-volatile residues—may accumulate at the substrate–perovskite interface or within grain boundaries during large-area processing, which could impede charge transport or induce recombination. Furthermore, the large ink volume and longer drying times in scalable methods can alter additive behaviour, require tailored formulations. Future research should focus volatile or migratory additives that facilitate crystallization control without leaving detrimental residues, as well as rheology-modifying additives that ensure ink stability and uniform wetting over substrate widths >10 cm. The search for ideal additives should also prioritize non-toxic, earth-abundant, and inexpensive materials to support the sustainable idea of perovskite photovoltaics, in addition to the potential impact of additive leaching.

Looking ahead, future additive engineering should advance beyond passive crystallization control toward the design of multifunctional molecules that can concurrently passivate ionic defects, enhance moisture resistance, improve interfacial charge transport, and suppress ion migration. A crucial transition from empirical discovery to rational design will be necessary, facilitated by the adoption of high-throughput computation and screening. One promising approach to quickly identifying next-generation additives is the use of artificial intelligence and machine learning to predict molecular structures that can interact with perovskite components in an efficient manner. For instance, Density functional theory (DFT) calculations can be employed to understand the oxidation pathways of

Sn^{2+} and the role of additives in inhibiting this process. The interaction energy between Sn^{2+} and potential Lewis base additives (e.g., acetates, phosphonates, or thiols) can be calculated to find molecules that strongly coordinate with Sn^{2+}, thereby minimize its reactivity with oxygen and moisture. Machine learning models can be trained on existing datasets of Sn-perovskite-additive interactions, which can predict new candidate molecules with desired characteristics. The key feature of such model can include electronic properties, molecular descriptors, binding energies with Sn^{2+}, I^-, and organic cations and, Solubility parameters and volatility. Such models can classify additives that simultaneously chelate Sn^{2+} to inhibit oxidation, alter crystallization kinetics for larger grains and increase hydrophobicity at grain boundaries. Finally, the field would benefit immensely from establishing more universal design rules that connect additive functional groups to specific crystallization outcomes. For example, Lewis base groups (e.g., C=O, $-NH_2$, -S=O, -CN) coordinate with Pb^{2+} or Sn^{2+} ions to form intermediate complexes that decelerate crystallization and passivate defects. Hydrophobic moieties (e.g., $-CF_3$, alkyl chains) enhance moisture stability by accumulating at grain boundaries. Hydrogen-bonding groups (-OH, -COOH) modulate crystallization kinetics and mitigate residual stress, while halide anions (Cl^-, Br^-) effectively stabilize crystal phases, passivate vacancies, and direct crystal orientation.

In conclusion, additive engineering offers the crucial scientific insights required to produce the high-quality films necessary for PSC commercialization. However, tackling these future obstacles through interdisciplinary cooperation will be key to translating laboratory success into durable, high-performance, and commercially viable perovskite solar technology.

Author Contributions

M.A.: Conceptualization, Formal Analysis, Investigation, Writing—Original Draft, Writing—Review & Editing. M.C.: Conceptualization, Formal Analysis, Supervision, Validation, Writing—Review & Editing, Material Support, Funding Acquisition. X.L.: Writing—Review & Editing, Funding Acquisition. X.C.: Writing—Review & Editing. Z.L.: Writing—Review & Editing A.T.: Writing—Review & Editing. All authors have read and agreed to the published version of the manuscript.

Funding

This work was sponsored by the National Natural Science Foundation of China (52202169 and 22279033), Special Foundation for Carbon Peak Carbon Neutralization Technology Innovation Program of Jiangsu Province (BE2022026), the Project for Young Foreign Experts (QN2023124001L), the Fundamental Research Funds for the Central Universities(2021PT012). the BRICS Framework Programme (52261145703).

Conflicts of Interest

The authors declare no conflict of interest.

References

1. Green, M.A.; Dunlop, E.D.; Yoshita, M.; et al. Solar cell efficiency tables (Version 64). *Prog. Photovolt. Res. Appl.* **2024**, *32*, 425–441.
2. Xu, J. USTC Set New Record in Perovskite Cell Efficiency. 2023. Available online: https://en.ustc.edu.cn/info/1007/4929.htm (accessed on 16 September 2024).
3. LONGI. LONGi Sets New World-Record for Silicon Solar Cell Efficiency, Launching 2nd Generation Ultra-Efficient BC-Based Module. 2024. Available online: https://www.longi.com/en/news/longi-hi-mo9-bc-world-record/ (accessed on 8 May 2024).
4. Liu, Z.; Ono, L.K.; Qi, Y. Additives in metal halide perovskite films and their applications in solar cells. *J. Energy Chem.* **2020**, *46*, 215–228.
5. Li, H.; Wu, G.; Li, W.; et al. Additive Engineering to Grow Micron-Sized Grains for Stable High Efficiency Perovskite Solar Cells. *Adv. Sci.* **2019**, *6*, 1901241.
6. Chen, J.; Kim, S.G.; Ren, X.; et al. Effect of bidentate and tridentate additives on the photovoltaic performance and stability of perovskite solar cells. *J. Mater. Chem. A Mater.* **2019**, *7*, 4977–4987.
7. Liu, C.; Tu, J.; Hu, X.; et al. Enhanced Hole Transportation for Inverted Tin-Based Perovskite Solar Cells with High Performance and Stability. *Adv. Funct. Mater.* **2019**, *29*, 1808059.
8. Yang, I.S.; Park, N. Dual Additive for Simultaneous Improvement of Photovoltaic Performance and Stability of Perovskite Solar Cell. *Adv. Funct. Mater.* **2021**, *31*, 2100396.
9. Si, H.; Liao, Q.; Kang, Z.; et al. Deciphering the NH_4PbI_3 Intermediate Phase for Simultaneous Improvement on Nucleation and Crystal Growth of Perovskite. *Adv. Funct. Mater.* **2017**, *27*, 1701804.

10. Li, T.; Pan, Y.; Wang, Z.; et al. Additive engineering for highly efficient organic–inorganic halide perovskite solar cells: Recent advances and perspectives. *J. Mater. Chem. A Mater.* **2017**, *5*, 12602–12652.
11. Patil, S.V.; Dave, S.; Bhargava, K. Comparative Analysis of $MAPbI_3$ and $FAPbI_3$ based Perovskite Solar Cells: A Numerical Evaluation. In *Proceedings of 28th National Conference on Condensed Matter Physics: Condensed Matter Days 2020 (CMDAYS20)*; Springer: Singapore, 2021; pp. 177–185.
12. Zheng, Z.; Wang, S.; Hu, Y.; et al. Development of formamidinium lead iodide-based perovskite solar cells: Efficiency and stability. *Chem. Sci.* **2022**, *13*, 2167–2183.
13. Cui, X.; Jin, J.; Tai, Q.; et al. Recent Progress on the Phase Stabilization of $FAPbI_3$ for High-Performance Perovskite Solar Cells. *Solar RRL* **2022**, *6*, 2200497.
14. Hu, H.; Singh, M.; Wan, X.; et al. Nucleation and crystal growth control for scalable solution-processed organic–inorganic hybrid perovskite solar cells. *J. Mater. Chem. A Mater.* **2020**, *8*, 1578–1603.
15. Bi, D.; Yi, C.; Luo, J.; et al. Polymer-templated nucleation and crystal growth of perovskite films for solar cells with efficiency greater than 21%. *Nat. Energy* **2016**, *1*, 16142.
16. Zhao, J.; Li, Z.; Wang, M.; et al. Exploring the film growth in perovskite solar cells. *J. Mater. Chem. A Mater.* **2021**, *9*, 6029–6049.
17. Liu, C.; Cheng, Y.B.; Ge, Z. Understanding of perovskite crystal growth and film formation in scalable deposition processes. *Chem. Soc. Rev.* **2020**, *49*, 1653–1687.
18. Ke, L.; Ding, L. Perovskite crystallization. *J. Semicond.* **2021**, *42*, 080203.
19. Yang, Y.; Xue, Z.; Chen, L.; et al. Large-area perovskite films for PV applications: A perspective from nucleation and crystallization. *J. Energy Chem.* **2021**, *59*, 626–641.
20. Wang, Z.; Zhu, Z.; Jin, J.; et al. Modulated crystal growth enables efficient and stable perovskite solar cells in humid air. *Chem. Eng. J.* **2022**, *442*, 136267.
21. Ma, Y.; Liu, N.; Zai, H.; et al. Amidinium additives for high-performance perovskite solar cells. *J. Mater. Chem. A Mater.* **2022**, *10*, 3506–3512.
22. Shi, X.; Chen, J.; Wu, Y.; et al. Efficient Formamidinium-Based Planar Perovskite Solar Cells Fabricated Through a CaI_2–PbI_2 Precursor. *ACS Sustain. Chem. Eng.* **2020**, *8*, 4267–4275.
23. Cao, Y.; Yan, N.; Wang, M.; et al. Designed Additive to Regulated Crystallization for High Performance Perovskite Solar Cell. *Angew. Chem. Int. Ed.* **2024**, *63*, e202404401.
24. Wang, X.; Sun, W.; Tu, Y.; et al. Lansoprazole, a cure-four, enables perovskite solar cells efficiency exceeding 24%. *Chem. Eng. J.* **2022**, *446*, 137416.
25. Wang, H.; Zhang, Z.; Wang, X.; et al. Phenyltrimethylammonium chloride additive for highly efficient and stable FAPbI3 perovskite solar cells. *Nano Energy* **2024**, *123*, 109423.
26. Wang, M.; Li, L.; Wang, J.; et al. Accelerating direct formation of α-FAPbl3 by dual-additives synergism for inverted perovskite solar cells with efficiency exceeding 26%. *Chem. Eng. J.* **2025**, *505*, 159056.
27. Yin, Y.; Zhang, S.; Zhou, L.; et al. Combining in-situ formed PbI2 passivation and secondary passivation for highly efficient and stable planar heterojunction perovskite solar cells. *Org. Electron.* **2022**, *100*, 106361.
28. Yang, J.A.; Xiao, A.; Xie, L.; et al. Precise control of PbI2 excess into grain boundary for efficacious charge extraction in off-stoichiometric perovskite solar cells. *Electrochim. Acta* **2020**, *338*, 135697.
29. Gao, Y.; Raza, H.; Zhang, Z.; et al. Rethinking the Role of Excess/Residual Lead Iodide in Perovskite Solar Cells. *Adv. Funct. Mater.* **2023**, *33*, 2215171.
30. Zhao, Y.; Ma, F.; Qu, Z.; et al. Inactive $(PbI_2)_2$ RbCl stabilizes perovskite films for efficient solar cells. *Science* **2022**, *377*, 531–534.
31. Luo, S.; Cao, S.; Zheng, T.; et al. Melamine holding PbI_2 with three “arms”: An effective chelation strategy to control the lead iodide to perovskite conversion for inverted perovskite solar cells. *Energy Environ. Sci.* **2025**, *18*, 2436–2451.
32. Wang, Y.; Cheng, Y.; Yin, C.; et al. Manipulating Crystal Growth and Secondary Phase PbI2 to Enable Efficient and Stable Perovskite Solar Cells with Natural Additives. *Nanomicro Lett.* **2024**, *16*, 183.
33. Dailey, M.; Li, Y.; Printz, A.D. Residual Film Stresses in Perovskite Solar Cells: Origins, Effects, and Mitigation Strategies. *ACS Omega* **2021**, *6*, 30214–30223.
34. Rolston, N.; Bush, K.A.; Printz, A.D.; et al. Engineering Stress in Perovskite Solar Cells to Improve Stability. *Adv. Energy Mater.* **2018**, *8*, 1802139.
35. Hu, S.; Duan, C.; Du, H.; et al. A stress relaxation strategy for preparing high-quality organic–inorganic perovskite thin films via a vapor–solid reaction. *J. Mater. Chem. A Mater.* **2023**, *11*, 23387–23396.
36. Zuo, G.; Zhu, P.; Zeng, J.; et al. Modulating Internal Residual Stress for Efficient and Durable Flexible Perovskite Solar Cells. *Solar RRL* **2025**, *9*, 2500052.
37. Sun, Q.; Tuo, B.; Ren, Z.; et al. A Thiourea Competitive Crystallization Strategy for FA-Based Perovskite Solar Cells. *Adv. Funct. Mater.* **2022**, *32*, 2208885.

38. Li, M.; Zhou, J.; Tan, L.; et al. Multifunctional succinate additive for flexible perovskite solar cells with more than 23% power-conversion efficiency. *Innovation* **2022**, *3*, 100310.
39. Fang, Z.; Yan, N.; Liu, S. Modulating preferred crystal orientation for efficient and stable perovskite solar cells—From progress to perspectives. *InfoMat* **2022**, *4*, e12369.
40. Li, B.; Shen, T.; Yun, S. Recent progress of crystal orientation engineering in halide perovskite photovoltaics. *Mater. Horiz.* **2023**, *10*, 13–40.
41. Xu, Z.; Gong, Y.; Wang, J.; et al. Carbon nanofibers fabricated via electrospinning to guide crystalline orientation for stable perovskite solar cells with efficiency over 24%. *Chem. Eng. J.* **2023**, *453*, 139961.
42. Li, M.; Sun, R.; Chang, J.; et al. Orientated crystallization of FA-based perovskite via hydrogen-bonded polymer network for efficient and stable solar cells. *Nat. Commun.* **2023**, *14*, 573.
43. Wu, Y.; Wang, Q.; Chen, Y.; et al. Stable perovskite solar cells with 25.17% efficiency enabled by improving crystallization and passivating defects synergistically. *Energy Environ. Sci.* **2022**, *15*, 4700–4709.
44. Kim, G.; Min, H.; Lee, K.S.; et al. Impact of strain relaxation on performance of α-formamidinium lead iodide perovskite solar cells. *Science* **2020**, *370*, 108–112.
45. Zhou, T.; Xu, Z.; Wang, R.; et al. Crystal Growth Regulation of 2D/3D Perovskite Films for Solar Cells with Both High Efficiency and Stability. *Adv. Mater.* **2022**, *34*, 2200705.
46. Zhong, H.; Liu, X.; Liu, M.; et al. Suppressing the crystallographic disorders induced by excess PbI2 to achieve trade-off between efficiency and stability for PbI2-rich perovskite solar cells. *Nano Energy* **2023**, *105*, 108014.
47. Li, Q.; Li, D.; Li, Z.; et al. Tailoring Crystal Growth Regulation and Dual Passivation for Air-Processed Efficient Perovskite Solar Cells. *Adv. Sci.* **2025**, *12*, 2407401.
48. Zhu, H.; Zhang, F.; Xiao, Y.; et al. Suppressing defects through thiadiazole derivatives that modulate $CH_3NH_3PbI_3$ crystal growth for highly stable perovskite solar cells under dark conditions. *J. Mater. Chem. A Mater.* **2018**, *6*, 4971–4980.
49. Liu, P.; Chen, Y.; Xiang, H.; et al. Benefitting from Synergistic Effect of Anion and Cation in Antimony Acetate for Stable $CH_3NH_3PbI_3$-Based Perovskite Solar Cell with Efficiency Beyond 21%. *Small* **2021**, *17*, 2102186.
50. Shi, X.; Wu, Y.; Chen, J.; et al. Thermally stable perovskite solar cells with efficiency over 21% via a bifunctional additive. *J. Mater. Chem. A Mater.* **2020**, *8*, 7205–7213.
51. Lee, J.W.; Kim, H.S.; Park, N.G. Lewis Acid–Base Adduct Approach for High Efficiency Perovskite Solar Cells. *Acc. Chem. Res.* **2016**, *49*, 311–319.
52. Xu, C.; Zhang, Z.; Zhang, S.; et al. Manipulation of Perovskite Crystallization Kinetics via Lewis Base Additives. *Adv. Funct. Mater.* **2021**, *31*, 2009425.
53. Cao, X.; Li, C.; Li, Y.; et al. Enhanced performance of perovskite solar cells by modulating the Lewis acid–base reaction. *Nanoscale* **2016**, *8*, 19804–19810.
54. Zhu, X.; Lin, R.; Gu, H.; et al. Ecofriendly Hydroxyalkyl Cellulose Additives for Efficient and Stable $MAPbI_3$-Based Inverted Perovskite Solar Cells. *Energy Environ. Mater.* **2023**, *6*, e12426.
55. Tao, J.; Wang, Z.; Wang, H.; et al. Additive Engineering for Efficient and Stable $MAPbI_3$-Perovskite Solar Cells with an Efficiency of over 21%. *ACS Appl. Mater. Interfaces* **2021**, *13*, 44451–44459.
56. Yang, Y.; Peng, H.; Liu, C.; et al. Bi-functional additive engineering for high-performance perovskite solar cells with reduced trap density. *J. Mater. Chem. A Mater.* **2019**, *7*, 6450–6458.
57. Mateen, M.; Arain, Z.; Liu, X.; et al. Boosting optoelectronic performance of $MAPbI_3$ perovskite solar cells via ethylammonium chloride additive engineering. *Sci. China Mater.* **2020**, *63*, 2477–2486.
58. Ouedraogo, N.A.N.; Chen, Y.; Xiao, Y.Y.; et al. Stability of all-inorganic perovskite solar cells. *Nano Energy* **2020**, *67*, 104249.
59. Chen, J.; Choy, W.C.H. Efficient and Stable All-Inorganic Perovskite Solar Cells. *Solar RRL* **2020**, *4*, 2000408.
60. Ma, T.; Wang, S.; Zhang, Y.; et al. The development of all-inorganic $CsPbX_3$ perovskite solar cells. *J. Mater. Sci.* **2020**, *55*, 464–479.
61. Patil, J.V.; Mali, S.S.; Hong, C.K. Reducing Defects of All-Inorganic γ-$CsPbI_2$ Br Thin Films by Ethylammonium Bromide Additives for Efficient Perovskite Solar Cells. *ACS Appl. Mater. Interfaces* **2022**, *14*, 25576–25583.
62. Kim, K.S.; Jin, I.S.; Park, S.H.; et al. Methylammonium Iodide-Mediated Controlled Crystal Growth of $CsPbI_2$ Br Films for Efficient and Stable All-Inorganic Perovskite Solar Cells. *ACS Appl Mater Interfaces* **2020**, *12*, 36228–36236.
63. Ren, Y.; Hao, Y.; Zhang, N.; et al. Exploration of polymer-assisted crystallization kinetics in $CsPbBr_3$ all-inorganic solar cell. *Chem. Eng. J.* **2020**, *392*, 123805.
64. Peng, H.; Cai, M.; Zhou, J.; et al. Structurally Reinforced All-Inorganic $CsPbI_2$ Br Perovskite by Nonionic Polymer via Coordination and Hydrogen Bonds. *Solar RRL* **2020**, *4*, 2000216.
65. Lü, J.; Huo, X.; Liu, W.; et al. Additive engineering by dicyandiamide for high-performance carbon-based inorganic perovskite solar cells. *Mater. Today Energy* **2024**, *44*, 101628.
66. Fu, S.; Wang, J.; Liu, X.; et al. Multifunctional liquid additive strategy for highly efficient and stable $CsPbI_2Br$ all-inorganic perovskite solar cells. *Chem. Eng. J.* **2021**, *422*, 130572.

67. Patil, J.V.; Mali, S.S.; Hong, C.K. Grain size enlargement and controlled crystal growth by formamidinium chloride additive-added γ-$CsPbI_2Br$ thin films for stable inorganic perovskite solar cells. *Mater. Today Chem.* **2022**, *26*, 101118.
68. Ayaydah, W.; Raddad, E.; Hawash, Z. Sn-Based Perovskite Solar Cells towards High Stability and Performance. *Micromachines* **2023**, *14*, 806.
69. Abate, A. Stable Tin-Based Perovskite Solar Cells. *ACS Energy Lett.* **2023**, *8*, 1896–1899.
70. Dong, H.; Ran, C.; Gao, W.; et al. Crystallization Dynamics of Sn-Based Perovskite Thin Films: Toward Efficient and Stable Photovoltaic Devices. *Adv Energy Mater.* **2022**, *12*, 2102213.
71. Li, F.; Hou, X.; Wang, Z.; et al. FA/MA Cation Exchange for Efficient and Reproducible Tin-Based Perovskite Solar Cells. *ACS Appl Mater Interfaces* **2021**, *13*, 40656–40663.
72. Tang, G.; Li, S.; Cao, J.; et al. Synergistic effects of the zinc acetate additive on the performance enhancement of Sn-based perovskite solar cells. *Mater. Chem. Front.* **2021**, *5*, 1995–2000.
73. Li, G.; Su, Z.; Li, M.; et al. Ionic Liquid Stabilizing High-Efficiency Tin Halide Perovskite Solar Cells. *Adv. Energy Mater.* **2021**, *11*, 2101539.
74. Su, Y.; Yang, J.; Liu, G.; et al. Acetic Acid-Assisted Synergistic Modulation of Crystallization Kinetics and Inhibition of Sn^{2+} Oxidation in Tin-Based Perovskite Solar Cells. *Adv. Funct. Mater.* **2022**, *32*, 2109631.
75. Jin, Z.; Zhang, Z.; Xiu, J.; et al. A critical review on bismuth and antimony halide based perovskites and their derivatives for photovoltaic applications: Recent advances and challenges. *J. Mater. Chem. A Mater.* **2020**, *8*, 16166–16188.
76. Ahmad, K.; Mobin, S.M. Recent Progress and Challenges in $A_3Sb_2X_9$-Based Perovskite Solar Cells. *ACS Omega* **2020**, *5*, 28404–28412.
77. Yang, Y.; Liu, C.; Cai, M.; et al. Dimension-Controlled Growth of Antimony-Based Perovskite-like Halides for Lead-Free and Semitransparent Photovoltaics. *ACS Appl. Mater. Interfaces* **2020**, *12*, 17062–17069.
78. Kim, E.B.; Akhtar, M.S.; Shin, H.S.; et al. A review on two-dimensional (2D) and 2D–3D multidimensional perovskite solar cells: Perovskites structures, stability, and photovoltaic performances. *J. Photochem. Photobiol. C Photochem. Rev.* **2021**, *48*, 100405.
79. Zhao, X.; Liu, T.; Loo, Y. Advancing 2D Perovskites for Efficient and Stable Solar Cells: Challenges and Opportunities. *Adv. Mater.* **2022**, *34*, 2105849.
80. Zhang, W.; Wu, X.; Zhou, J.; et al. Pseudohalide-Assisted Growth of Oriented Large Grains for High-Performance and Stable 2D Perovskite Solar Cells. *ACS Energy Lett.* **2022**, *7*, 1842–1849.
81. Wang, Z.; Liu, L.; Liu, X.; et al. Uncovering synergistic effect of chloride additives for efficient quasi-2D perovskite solar cells. *Chem. Eng. J.* **2022**, *432*, 134367.
82. Yang, Y.; Liu, C.; Mahata, A.; et al. Universal approach toward high-efficiency two-dimensional perovskite solar cells via a vertical-rotation process. *Energy Environ. Sci.* **2020**, *13*, 3093–3101.
83. Yu, S.; Meng, J.; Pan, Q.; et al. Imidazole additives in 2D halide perovskites: Impacts of -CN vs. $-CH_3$ substituents reveal the mediation of crystal growth by phase buffering. *Energy Environ. Sci.* **2022**, *15*, 3321–3330.